JBC Papers in Press. Published on May 31, 2017 as Manuscript M117.786491
The latest version is at http://www.jbc.org/cgi/doi/10.1074/jbc.M117.786491

Microtubule assisted altered trafficking of Astrocytic Gap Junction Protein Connexin 43 is associated with depletion of Connexin 47 during Mouse Hepatitis Virus infection

Rahul Basu, Abhishek Bose, Deepthi Thomas and Jayasri Das Sarma*

Department of Biological Sciences, Indian Institute of Science Education and Research Kolkata, Mohanpur-741246, India

Running title: Gap junction alteration during viral infection

*To whom correspondence should be addressed: Jayasri Das Sarma; Department of Biological Sciences; Indian Institute of Science Education and Research (IISER) Kolkata; India. E-Mail: dassarmaj@iiserkol.ac.in. Phone: +91-9748642423. Fax: +91-33-2587 3028

Keywords: connexin, gap junction, multiple sclerosis, tubulin, mouse hepatitis virus

Abstract

Gap junctions (GJs) are important for maintenance of central nervous system (CNS) homeostasis. GJ proteins, connexin 43 (Cx43) and connexin 47 (Cx47), play crucial role in production and maintenance of central nervous system (CNS) myelin. Cx43 is mainly expressed by astrocytes in the CNS, and forms gap junction intercellular communications (GJICs) between astrocytes (Cx43/Cx43) and astrocytes to oligodendrocytes (Cx43/Cx47). Mutations of these connexin (Cx) proteins cause dysmyelinating diseases in humans. Previously it has been shown that Cx43 localization and expression is altered due to mouse hepatitis virus (MHV)-A59 infection both *in vivo* and *in vitro*; however, its mechanism and association with loss of myelin protein was not elaborated. Thus, we explored potential mechanisms by which MHV-A59 infection alters Cx43 localization, and examined effects of viral infection on Cx47 expression and its association with loss of myelin marker proteolipid protein (PLP). Immunofluorescence and total internal reflection fluorescence (TIRF) microscopy confirmed that MHV-A59 used microtubules (MTs) as a conduit to reach the cell surface and restricted MT mediated Cx43 delivery to cell membrane. Co-immunoprecipitation experiments demonstrated that Cx43/β-tubulin molecular interaction was depleted due to protein-protein interaction between viral particles and MTs. During acute MHV-A59 infection, oligodendrocytic Cx47, which is mainly stabilized by Cx43 *in vivo*, was downregulated, and its characteristic staining remained disrupted even at chronic phase. The loss of Cx47 was associated with loss of PLP at the chronic stage of MHV-A59 infection.

Introduction

Microtubules (MTs) are components of the cytoskeleton that consist of polymers of α and β-tubulins. Highly dynamic structures of MTs spontaneously undergo phases of polymerization and catastrophe, and play major roles in various cellular processes. These processes include intracellular transportation of organelles and molecules. The movement and delivery of proteins, vesicular carriers and the organelles from their site of production to specific destinations are crucial for their function. Hence, the trafficking of different membrane proteins like cell junction proteins and signaling molecules to the cell membrane plays an essential role for cellular functioning. A group of cell junction proteins, gap junctions (GJs) form intercellular channels between two neighboring cells only after successful delivery and docking to the cell membrane. GJs are made up of connexin (Cx) proteins, which are synthesized in the endoplasmic reticulum (ER), oligomerized in intercellular organelles like ER or the trans-Golgi network

(TGN), and finally delivered to the cell surface (1) and a pair of hemichannels from a GJ plaque.

, Cx43 is mainly expressed by astrocytes (2), which forms homotypic Cx43/Cx43 mediated channels with other astrocytes, and heterotypic Cx43/Cx47 mediated channels with oligodendrocytes (3). These channels are important for maintaining CNS nutrient homeostasis, ionic buffering and small molecule (< 1 kD) exchange (4-9). Astrocytes also express Cx30 and Cx26, which form gap junction intercellular communication (GJIC) with other cells in panglial cells but are not redundant for Cx43 expression and function (10-12). A number of recent studies examined mechanistic details of Cx43 delivery to the cell surface. Delivery of Cx43 specifically relies on the MT network. Cx43 molecules are delivered in vesicular carriers which traffic along MTs from the Golgi to the plasma membrane (13). The delivery of Cx43 containing vesicles involves intermediate proteins like EB1, p150 (glued) of dynein/dynactin complexes, and β-catenin (14). Cx43 molecules are also known to bind MTs at the cell surface (15).

It has been shown that viral infections such as Rous sarcoma virus (RSV), Borna disease virus (BDV), and human influenza virus can alter Cx43 expression *in vivo* or *in vitro*, but the mechanism of Cx43 alteration remains elusive (16-18). Our recent study showed that a neurotropic demyelinating strain of mouse hepatitis virus (MHV)-A59 causes retention of Cx43 in the endoplasmic reticulum/ endoplasmic reticulum Golgi intermediate complex (ER/ERGIC), affecting functional channel formation between primary astrocytes, and reduces Cx43 expression in mouse brain (19), but the molecular mechanism of Cx43 retention in the ER/ERGIC, was not described. For efficient infection and cell-to-cell spread, many viruses have developed mechanisms for utilizing cytoskeletal elements. The JHM strain of mouse hepatitis virus (MHV) uses MTs for transneuronal spread within the CNS, and the viral nucleocapsid (N) protein is predicted to have MT interactive properties (20). A recent study shows a demyelinating recombinant strain of MHV, RSA59, uses the MT network as a conduit for cell-to-cell spread (21). Other viruses like Herpes simplex virus 1 (HSV-1) utilize the cellular MT

One of the most studied Cx, Cx43, is expressed in multiple organs including CNS, heart and lungs. In the CNS network for trafficking of virions and viral glycoproteins to virus release sites (22). Vaccinia virus is reported to use both MT networks and actin filament for egression (23). Adenovirus entry to host cells is dependent on MTs (24) and the virus also uses MT associated molecular motors for retrograde transport (25). The adeno-associated virus (AAV) also displays unidirectional movement on MTs toward the nuclei (26). In contrast, there are few studies available delineating which specific molecules, if any, exhibited altered intracellular localization due to MT mediated viral trafficking. Thus, our current study is designed to understand whether specific utilization of the MT network for virus trafficking by MHV-A59 may be an underlying mechanism by which Cx43 is restricted from localizing to the cell surface.

MHV-A59 causes hepatitis and meningoencephalitis in the acute phase of infection, and leads to demyelination and concurrent axonal loss during the chronic phase, serving as a virus-induced chronic progressive model of the human CNS demyelinating disease, multiple sclerosis (MS) (27,28). Cx43 mediated gap junction intercellular communications (GJICs) play a critical role in formation and maintenance of normal myelin. Recent studies indicate that GJIC formation between astrocytic Cx43 and oligodendrocytic Cx47 are crucial for human myelination (29,30). These GJICs are important in K+ buffering and nutrient homeostasis (31). Upon docking, Cx47 GJ hemichannels are phosphorylated and stabilized as GJ plaques by Cx43 (32). Hence, alteration of Cx43 expression and trafficking is hypothesized to have critical impact on Cx47 expression in this viral model of neuroinflammation. Altered Cx43/Cx47 mediated heterotypic GJIC formation between astrocytes and oligodendrocytes could be associated with loss of myelin protein. In this context, we extended our study to examine alterations of Cx47 during MHV-A59 infection and its association with myelin marker proteolipid protein (PLP).

In summary, the current study was focused on understanding the molecular mechanisms of virus-

induced alteration of Cx43. This study was also extended to understand whether the alteration of Cx43 was also associated with altered oligodendrocytic GJ and myelin protein expression. The prior studies in this field showed that the MT network is important for trafficking of Cx43 as well as viral particles. In this context, we observed that colocalization between Cx43/β-tubulin was reduced due to viral infection and in the same time, viral particles colocalized with the MT network. Upon MHV-A59 infection, the delivery of Cx43 to the cell surface, along MT threads, was reduced. At the molecular level, Cx43/β-tubulin protein-protein interaction was reduced and it was confirmed that MHV-A59 interacted with MTs. In addition, Cx47 was depleted in MHV-A59 infected mouse brain, and this GJ alteration was associated with loss of myelin protein PLP.

Results

Localization of Cx43 upon colchicine treatment

Primary astrocytes were treated with 100μM colchicine for 24 h as a representative dose to disrupt the MT network without affecting cell viability. The cell viability of primary astrocytes, upon colchicine treatment, is shown in supplementary fig. S1. Control cells were maintained in parallel. Cells were coimmunostained with rabbit anti-Cx43 antisera (red) and mouse anti-β-tubulin antisera (green). Z-stacking was obtained by confocal microscope, with signals obtained from the base of the cells (Fig. 1 plane 1) to the medial part of the cells (Fig. 1 plane 4), to observe the distribution of Cx43 upon MT disruption. Untreated cells showed presence of Cx43 at the basal stack (thin arrow: Fig. 1 A) and peripheral part of the medial stacks of cells (Fig. 1 B, C, D). In contrast, at the basal stack of colchicine treated cells (thick arrow: Fig. 1 E), presence of Cx43 was diminished, whereas the medial stacks showed continued presence of Cx43 mostly inside the cells (thick arrow: Fig. 1 F, G, H), suggesting Cx43 delivery to cell surface was restricted upon MT disruption. This was confirmed by disrupted β-tubulin staining (Fig. 1 F, G, H). Digitally magnified insets (Fig. 1 I, J) show that Cx43 was present on MT threads with an appearance of "beads-on-a string" in a single focal plane. Colocalization was evident, specifically where intensity of Cx43 and β-tubulin was similar (ring-like yellow spots, thin arrow: Fig. 1 I). Colchicine treated cells showed smear-like disruption of β-tubulin signal, whereas Cx43 surface localization and colocalization with MT was restricted (thick arrow: Fig. 1 J). For better understanding of Cx43 and tubulin localization, individual channel images of each plane of untreated and colchicine treated cells are shown in supplementary fig. S2.

Reduction of Cx43/β-tubulin colocalization due to virus infection and colocalization of viral particles with β-tubulin.

Cx43 molecules are reported to directly bind to MTs (15), and the MT network helps direct delivery of Cx43 hemichannels to the cell surface (14). Primary astrocytes were infected with MHV-A59 and mock infected cells were maintained in parallel. After 24 h p.i., cells were cytofixed and subjected to double immunofluorescence with monoclonal anti-β-tubulin (green: Fig. 2 A, E, I) and polyclonal anti-Cx43 (red: Fig. 2 B, F, J) antibodies. Cells were counterstained with DAPI (blue). Both mock- and virus-infected cells showed normal MT morphology (Fig. 2 A, E), whereas, 100 μM colchicine treatment disrupted MT network (Fig. 2 I). Characteristic punctate staining of Cx43 was observed for mock-infected cells (Fig. 2B). Virus-infected (Fig. 2 F) and colchicine-treated cells (Fig. 2 J), showed intracellular localization of Cx43. Consistent with prior studies, primary astrocytes showed a proximal association between Cx43 and the MT network (thin arrow) (Fig. 2C). When the astrocytes were infected with MHV-A59, Cx43 was localized in a perinuclear compartment, with minimal association with the MT network (thick arrow: Fig. 2 G).Colchicine-treated cells showed a disrupted MT network and Cx43 staining was mainly redistributed in the cytosol (thick arrow: Fig. 2 K). The number of points containing colocalization of immunostaining and the intensity of staining was maximal for mock-infected cells (Fig. 2 D). Upon virus infection (Fig. 2 H) or microtubule disruption with colchicine (Fig. 2 L), colocalization was reduced. There was approximately 62.8 % reduction in colocalized staining within virus-infected cells compared to

mock-infected cells (**, P<0.01, Mann-Whitney U test) and approximately 80.3 % reduction in colchicine-treated cells compared to mock-infected cells (**, P<0.01, Mann-Whitney U test). Kruskal-Wallis analysis showed the differences in a three-way comparison of groups were statistically significant (****, P<0.0001). Five different images from N=3 biological replicates were quantified for each experimental group (Fig. 2 M). A staining intensity profile was drawn in digitally magnified images, which showed Cx43 molecules were present along a MT thread (Fig. 2 N, O), whereas Cx43 retained in the intracellular compartment in MHV-A59-infected cells did not show such alignment (Fig. 2 P, Q). Cx43 molecules showed high intensity peaks on MT threads in mock-infected cells (Fig. 2 R, S), but not in virus-infected cells (Fig. 2 T, U).

When mock-infected and virus-infected cells were similarly stained with monoclonal anti-viral- N (green: Fig. 3 A, D) and polyclonal anti-β-tubulin (red: Fig. 3 B, E) antibodies, similar tubulin morphology was observed for both. Maximum intensity projection (mip) images, obtained from an apotome microscope, showed dispersion of viral staining from the perinuclear compartment to the cell periphery. Viral-N signal colocalized with β-tubulin staining, specifically noticeable at the cell surface (arrow: Fig. 3 F).As expected, no viral antigen was present in the mock-infected cells (Fig. 3 C).

Kinetics of viral spread in primary astrocytes and colocalization with MT network.

To examine whether viral particles were spreading along the MT network, primary astrocytes were mock- (Fig. 4 A, B) or MHV-A59-infected and at 6 h (Fig. 4 C, D), 12 h (Fig. 4 E, F), 18 h (Fig. 4 G, H) and 24 h (Fig. 4 I, J) p.i., cells were labeled for β-tubulin (red) and viral-N (green). The amount of viral-N staining increased from 6 h p.i. to 24 h p.i. At 6 h and 12 h p.i., discrete viral particles were observed to be present on the MT-threads (Fig. 4 C, E: arrow and inset) and colocalization points were mainly located at the cell periphery (Fig. 4 D, F). Later, at 18 h and 24 h p.i., anti-N signal was more dispersed throughout the whole cell, and towards the cell border viral particles were localized on MTs (Fig. 4 G, I: arrow and inset). The number of colocalization points increased visually and were mainly located at the cell periphery and cell-to-cell junctions (Fig. 4 H, J).The number of spots containing colocalization of staining were counted, and plotted against increasing time p.i., which showed the number of colocalization spots increased from 6 h p.i. to 12 to 18h p.i. and reached its maximum at 24 h p.i. (**, P<0.01 for 6 h, 12 h and 18 h p.i. and 24 h p.i. each compared with mock by Mann-Whitney U test). ANOVA was performed by Kruskal-Wallis testing confirmed the variations between groups were significant (***, P<0.001). Five different fields were obtained from each experimental group in N=3 experiments (Fig. 4 K).

Confirmation of altered Cx43/β-tubulin colocalization at cell surface was due to viral particle/ β-tubulin association.

To understand the Cx43 and β-tubulin interaction at the cell membrane, total internal reflection fluorescence (TIRF) microscopy was performed, which specifically magnifies staining of molecules present at or in close proximity (100 nm) to the cell surface. Cells plated on glass coverslips were mock- or virus-infected, subjected to double immunofluorescence for Cx43 (green: Fig. 5 A, F) and β-tubulin (red: Fig. 5 B, G), and nuclei were stained with DAPI (blue). Cx43 was subjected to TIRF microscopy, keeping the imaging depth restricted to 100 nm. The whole cell MT network was captured by epifluorescence microscopy. In mock-infected astrocytes, TIRF images showed signal of Cx43 exclusively present at or near to the cell surface (Fig. 5A, C). In contrast, MHV-A59-infected cells showed minimal surface expression of Cx43 (Fig. 5F, H). MT morphology appeared normal in mock-infected and MHV-A59-infected cells (Fig. 5 B, C and G, H). In mock-infected cells, merged TIRF images showed that Cx43 molecules were closely associated with tubulin threads (thin arrow: Fig. 5C), and indeed aligned along the MT threads (inset, thin arrow: Fig. 5 D) or positioned at the tip of the MT threads (inset, thin arrow: Fig. 5 E). MHV-A59-infected astrocytes showed absence of MT-associated Cx43 signal near to the cell surface (Fig. 5 H). Insets showed that Cx43 molecules were restricted from reaching the cell surface (no TIRF signal was

detected, thick arrow: Fig. 5 I) and Cx43/β-tubulin association was lost (thick arrow: Fig. 5 J).

The loss of Cx43/β-tubulin colocalization was predicted to be due to association between viral particles and the MT network. Hence, cells were double immunolabeled for viral-N (green: Fig. 5 K, O) and β-tubulin (red: Fig. 5 L, P), and nuclei were stained with DAPI (blue). Mock-infected astrocytes showed no specific N-staining (Fig. 5 K), whereas, MHV-A59-infected cells showed profuse N expression (arrow: Fig. 5 O). The MT network appeared normal in both mock- and virus-infected cells (Fig. 5 L, P). High magnification (100 X) TIRF images were captured specifically for single infected cells, where viral spread at the surface was evident. In contrast to merged images for mock-infected cells (Fig. 5 M), viral particles were observed to be colocalized with MT signal (Fig. 5 Q). In digitally magnified insets viral particles were observed to be aligned along the MT thread at the cell surface, confirming that Cx43/MT association could be replaced by MHV-A59/MT association (Fig. 5 R). No viral-N staining was observed in the inset (Fig. 5 N).

For Cx43 localization, compared to MT-network, TIRF microscopy was used to capture the signal of Cx43 residing near cell surface (near 100 nm) and parallel epifluorescence images were captured for the same field. Cx43 was observed to be present in profuse amount as its characteristic punctate stain of Cx43 (Fig 6. thin arrow: A, merged: C). In contrast, MHV-A59 infected astrocytes showed mainly perinuclear localization of Cx43 (Fig 6. thick arrow: D, merged: F), which was not observed by TIRF imaging. MT morphology is shown for mock (Fig 6. B) or MHV-A59 infected cells (Fig. 6 E). The distance of Cx43 molecules from the nuclear centroid was measured with the help of imageJ (Fig. 6 G). For mock infected cells Cx43 was present approximately 25.9 μm away, which was reduced to approximately 12.7 μm in MHV-A59 infected cells. Data was obtained from nine different images from N= 3 biological replicates and average ± SD is represented in the graph (****, P<0.0001, t-test).

Altered protein-level interaction between Cx43 and β-tubulin upon MHV-A59 infection

To investigate the direct interaction between β-tubulin and Cx43, same number of primary astrocytes were mock-infected or infected with MHV-A59. Cells were lysed in non-denaturing condition; mouse monoclonal anti-β-tubulin antibody was used to immunoprecipitate β-tubulin, with the help of anti-mouse MagnaBind antibody. The sample was further denatured with Laemmli's buffer and was probed by rabbit polyclonal anti-Cx43 antibody (detectable nearly at 43 kDa). Uninfected primary astrocytes showed Cx43 was co-immunoprecipitated with β-tubulin and this interaction was significantly reduced upon MHV-A59 infection. Five percent input of the total extract showed there was a reduction of total Cx43 , upon virus infection but the expression of internal control γ-actin (detectable nearly at 42 kDa) was similar. The beads, without any primary antibody, showed no non-specific interaction in immunoprecipitation (Fig. 7 A). Densitometric analysis showed that Cx43, bound to β-tubulin, was reduced ~ 44.25 % in MHV-A59 infected cells, compared to the mock-infected cells (Fig. 7 B; ****, P<0.0001, t-test, n=3).

The reduction in Cx43/β-tubulin interaction was verified with the help of reverse co-IP, where proteins extracted in non-denaturing condition from both mock- and MHV-A59-infected astrocytes, were immunoprecipitated with polyclonal anti-Cx43 antibody and probed with monoclonal anti-β-tubulin antibody (detected nearly at 50 kDa). As expected, the expression of β-tubulin was similar between mock- and MHV-A59-infected cells. Loading of the beads showed no non-specific binding. Upon co-IP, there was a substantial reduction in β-tubulin signal, which was bound to Cx43 in virus-infected cells, compared to control cells (Fig. 7 C). There was an approximate 55.61 % reduction in β-tubulin/Cx43 interaction, demonstrated by Densitometric analysis (Fig. 7 D; ****, P<0.0001, t-test, n=3).

Interaction between viral particles and β-tubulin in MHV-A59 infected primary astrocytes

Primary astrocytes were mock- or MHV-A59-infected at an MOI of 2 and proteins were extracted in non-denaturing condition. Polyclonal anti-β-tubulin antibody was used to

immunoprecipitate β-tubulin and associated proteins. The samples were denatured and probed for viral-N by western blot using mouse monoclonal anti-N antibody, which is detectable nearly at 50 kDa. Samples showed similar amounts of γ-actin expression, whereas anti-N was detected only in samples from MHV-A59-infected cells but not in mock-infected ones. As expected, no nonspecific binding with the beads was observed. Anti-N signal was observed upon co-IP of β-tubulin in the infected astrocytes, suggesting that viral particles were interacting with the MT-network (Fig. 8).

Inhibition of dynein affected Cx43 delivery to cell surface

A small-molecule dynein inhibitor, ciliobrevin D (33), was used to block dynein in primary astrocytes upon treatment at 30, 50 and 100 μM concentration for 24 h, and untreated cells were maintained in parallel. Cells were immunolabeled with β-tubulin (green: Fig. 9 A-D), Cx43 (red: Fig. 9 A-D) and nuclei were counterstained with DAPI (blue). Mock-infected cells showed normal punctate appearance of Cx43 at the cell surface (thin arrow: Fig. 9 A). Ciliobrevin D treatment induced clustering of Cx43 inside primary astrocytes (thick arrow: Fig. 9 B-D), depleting the delivery of Cx43 at the cell surface. Dose dependent treatment of ciliobrevin induced localization of Cx43 aggregates around the nucleus, suggesting that dynein might have played a crucial role in altered MT mediated Cx43 trafficking to the cell surface.

Persistent loss of oligodendrocytic Cx47 due to MHV-A59 infection in mouse brain

Cx43 is reported to form heterotypic GJ plaques with oligodendrocytic partner Cx47, and also phosphorylates and stabilizes Cx47 in vivo (32). In MHV-A59 infection, whether the coupling partner of Cx43, oligodendrocytic Cx47 was altered or not, was examined at the total protein level. C57Bl/6 mice were either mock- or MHV-A59-infected and sacrificed at day 5 p.i. (acute infection phase) and at day 30 p.i. (chronic phase).Total protein was extracted from mouse brain and Cx47 expression (detectable nearly at 47 kDa) was compared by western blot. γ-actin (detected nearly at 42 kDa) was probed as internal control. In whole brain protein, Cx47 levels were reduced at the peak of inflammation at day 5 p.i., whereas γ-actin expression was similar in both mock- and MHV-A59-infected brains (Fig. 10 A). A croos-reactive signal is observed near 51 kDa for Cx47 western blot, as it was seen earlier in the previous reports also (34-36). The densitomeric analysis confirmed reduction in Cx47 expression, showing ~ 32.78 depletion of Cx47 signal, upon virus infection (Fig. 10 B, ***, $P<0.001$, t-test). At day 30 p.i. (peak of demyelination), Cx47 levels remained depleted in MHV-A59-infected brains, compared to similar expression of γ-actin in all brains (Fig. 10 C). There was a significant ~ 35.83 % reduction of Cx47, which sustained till the peak of demyelination (Fig. 10 D, ****, $P<0.0001$, t-test).

***In situ* expression of Cx47 in MHV-A59 infected mouse brain**

To verify whether loss of Cx47 measured in protein extracts from MHV-A59-infected brains was also detectible in situ, mock- and MHV-A59-infected mouse brains were subjected to cryosectioning and double label-immunofluorescence for viral-N (green: Fig. 11 A, E, I) and Cx47 (red: Fig 11 B, F, J). Nuclei were counterstained with DAPI (blue). At day 5 p.i., MHV-A59 infection was observed in mouse brain (Fig. 11 E), whereas mock-infected brain (Fig. 11 A) as well as day 30 p.i. MHV-A59-infected brain (Fig. 11 I) showed no viral-N signal. Cx47 showed characteristic signal at perikarya in mock-infected brains (thin arrow: Fig. 11 B). Characteristic Cx47 signal was disrupted in MHV-A59-infected brain (thick arrow: Fig. 11 F). This depletion of Cx47 perikaryonic signal was sustained at day 30 p.i. (Fig. 11 J). Merged images show prominent Cx47 puncta at oligodendrocytic somata and proximal processes without infection (Fig. 11 C), whereas depletion and degradation of Cx47 was observed around infected brain regions at day 5 p.i. (Fig. 11 G) and this depletion remained noticeable at day 30 p.i. when no productive viral infection was observed (Fig. 11 K). Digitally magnified insets for Cx47 show numerous Cx47 puncta distributed in a perikaryonic fashion (Fig. 11 D). The number as well as characteristic staining pattern of Cx47 puncta was depleted at day 5 p.i. (Fig. 11 H) and this loss was sustained at day 30 p.i. (Fig. 11 L).

Images (with an area of 135µm × 135µm) obtained from N=3 biological replicates were quantified for presence of complete perikaryonic punctate signal or disrupted signal of Cx47 (Fig. 11 M). A reduction of perikaryonic signal was observed for both at day 5 and day 30 p.i. At day 5 p.i., MHV-A59 infected mice showed ~ 7.567 number of Cx47 perikaryonic plaques were reduced in an area of 135µm × 135µm (***, P< 0.001, t-test) and at day 30 p.i., this depletion was ~ 6.9 intact Cx47 plaques in an area of 135µm × 135µm (**, P< 0.01, t-test) (Fig. 11 M).

Association of disrupted Cx47 signal with myelin marker PLP.

Ablation of Cx47 is reported to be associated with loss of myelin. Hence, mouse brain sections were similarly immunostained for Cx47 (green: Fig 12 A, E, I, M, Q, U) and myelin marker PLP (red: Fig. 12 B, F, J, N, R, V) and nuclei were stained with DAPI (blue). In mock-infected brains, Cx47 expression was profuse and perikaryonic. Cx47 was most abundant in and around white matter regions including corpus callosum (Fig. 12 A), anterior commissure (Fig. 12 I) and deep cerebellar white matter (Fig. 12 Q). Prominent PLP expression was observed in these regions of mock-infected brain (Fig. 12 B, J, R), where myelinated axon fibers were associated with normal Cx47 staining at oligodendrocyte somata (Fig. 12 C, K, S). Upon infection with MHV-A59, at day 30 p.i., prominent loss of characteristic Cx47 signal was observed in corpus callosum (Fig. 12 E), but in anterior commissure (Fig. 12 M) and deep cerebellar white matter (Fig. 12 U) only marginal loss in number and disrupted perikayonic signal of Cx47-positive puncta was observed. In these brains, loss of PLP signal was specifically observed in corpus callosum (Fig. 12 F) and marginal loss of PLP signal was observed in anterior commissure (Fig. 12 N) and cerebellum (Fig. 12 V). The prominent loss of Cx47 in corpus callosum was associated with loss of PLP (Fig. 12 G), whereas, in other regions, the alteration was marginal (Fig. 12 O, W). Digitally magnified insets show that in mock-infected brains, perikaryonic Cx47 signal was arranged in a "pearls-on-a-string" fashion around myelinated fibers (thin arrow: Fig. 12 D, L, T). In MHV-A59-infected brains, characteristic Cx47 staining was diminished around the degenerated myelin fibers in corpus callosum (thick arrow: Fig. 12 H) and the number of Cx47-puncta was reduced in and around other myelinated regions (Fig. 12 P, X) also.

Discussion

The current studies demonstrate two main, novel findings. First, MHV-A59 infection altered Cx43 trafficking to the cell surface in a MT-dependent manner. We report that MHV-A59 association with the MT network restricted Cx43 trafficking to the cell membrane. Second, the oligodendrocytic GJ coupling partner of Cx43, Cx47, was downregulated in MHV-A59 infection and this depletion was associated with loss of the myelin marker PLP at the chronic stage of viral infection.

The MT network is known to perform important functions in bidirectional transport within the cell. endoplasmic reticulum Golgi intermediate complex (ERGIC) structures move from ER exit sites to the Golgi by tracking along MTs (37), and vesicles emerging from Golgi reach the cell surface with the help of the same cytoskeletal network. As a result, trafficking of Cx43 molecules residing in these organelles was inhibited, preventing Cx43 from reaching the cell surface due to MT depolymerization induced by colchicine treatment. In contrast, in normal primary astrocytes Cx43 did localize at the cell periphery and was organized in a "beads-on-a-string" array on MT threads. Results suggest Cx43 molecules directly bind to β-tubulin at the cell surface, where it anchors MTs at their distal ends (15). Inside the cytoplasm, Cx43 molecules are reported to be associated with MTs plus the tracking protein EB1, which in turn, interacts with p150 (Glued). This glued protein is a component of the dynein/dynactin complex, and this complex can tether microtubules to adherens-junctions (AJs), resulting in the delivery of Cx43 at the cell surface (14). Similarly, in control primary astrocytes in the current studies it was observed that Cx43 was aligned along the MTs. Upon infection, this alignment was perturbed, and colocalization of Cx43-β-tubulin was significantly reduced. Interestingly, at the same time, viral particles were observed to be colocalized with the

MT network, specifically at the cell periphery. In early time of infection (6 and 12 h p.i.), colocalization was mostly observed at the distal parts of the cells. Interestingly, at 18 and 24 h p.i., the colocalization points were more spread out, with a drastic increase in colocalization at 24 h p.i. The distribution of colocalization points between viral-N and β-tubulin near the cell periphery, suggests that the organelle carriers containing Cx43 might be in dynamic, competitive interaction with trafficking viral particles for MTs. These findings were further supported by TIRF microscopy showing the presence of the viral particles residing at the vicinity of the cell surface. HSV-1 also uses MTs for the trafficking of virions, based on TIRF microscopy showing that these virions were clustered at specific sites along the adherent cell surface (22). Similarly, in the current study, MHV-A59 particles were confirmed to be aligned along the MTs, specifically at the periphery (near 100 nm). At the surface of uninfected astrocytes, Cx43 was observed to be associated along the same conduit. In contrast, in MHV-A59-infected cells, presence of Cx43 was not detected at the vicinity of cell surface, by TIRF microscopy, thus providing further evidence to suggest that viral particles used the MT network as a conduit to reach to the cell surface, replacing the Cx43 molecules.

Previous studies showed that another demyelinating strain of MHV, JHM, specifically uses the MT network for transneuronal spread and viral protein trafficking (20). Previous studies have also demonstrated that cytoskeletal molecules like actin filaments or MTs are exploited by various viruses to promote entry or spread from cell to cell. A rotavirus membrane glycoprotein, NSP-4, binds to MTs and arrests normal ER-to-Golgi trafficking (38). Ebola Virus Matrix Protein VP40 is reported to interact directly with MTs (39). Although multiple studies show direct or indirect interaction of virus with MTs, there is limited data available on the specific cellular proteins that might be disrupted due to MT mediated viral trafficking. The co-IP experiment performed here, confirmed that the molecular interaction between Cx43 and β-tubulin was significantly diminished upon viral infection. Co-IP with β-tubulin and N-protein demonstrated biochemical evidence of direct interaction of virus with the MT network. Taken together, the phenomenon of viral interaction with MTs and transport along MTs might be an important mechanism of the normal cell-to-cell propagation pathway of MHV-A59. To the best of our knowledge, this is the first report which showed MT network mediated trafficking of MHV-A59 directly affecting trafficking of Cx43 molecules to the cell surface.

While this study showed that MHV-A59 interacted with MTs and downregulated interaction between Cx43 and β-tubulin, it is feasible that one or more accessory proteins are also involved in this interaction. Prior studies suggested that the dynein/dynactin complex has an important role in Cx43 trafficking. It has also been shown that negative stranded RNA virus, Hantaan virus, nucleocapsid protein uses MTs for intracellular trafficking and the movement occurs via molecular motors such as dynein (40). In addition, during adenovirus infection, cytoplasmic dynein is reported to mediate interaction between viral capsid and MTs (25). Thus, there may be a crucial role of molecular motors and other MT-associated proteins involved in altered trafficking of Cx43.This is supported by the current studies, where the inhibition of cytoplasmic dynein by ciliobrevin D resulted in impaired delivery of Cx43 to the cell surface. Hence, further investigation is warranted to determine the specific molecular motors involved in transport of virus that may mediate retention of Cx43 in the ER/ERGIC.

In contrast to other Cxs, Cx43 is specifically known to interact with tubulins (15). There are other studies available that show Cx26 is highly dependent on the MT network for GJ formation, compared to partial dependence of cell surface delivery of other Cxs, like Cx32 and Cx43 (41). In addition, nocodazole induced destabilization of the MT network also affected Cx30 mediated GJ plaque formation, proving its partial dependency on MTs for delivery to the cell surface (42). Astrocytes are reported to express Cx30 and Cx26, along with a major expression of Cx43 (43). Hence, whether MHV-A59 infection also disrupts MT-dependent transport of other astrocytic connexins can be an important focus of future.

This study provides important information about the interaction between the MT network and MHV-A59, and results support its direct involvement in diminishing Cx43 specific GJIC formation. MHV-A59 induced neuroinflammation in the acute stage of infection leads to demyelination and axonal loss in the chronic stage (28). MHV infection produces persistent, productive infection in primary astroglial cell cultures but the pathological importance of glial cell infection remains unclear (44). Meningeal fibroblasts also express a large amount of Cx43 (45). Virus infection might therefore also disrupt glia/meningeal fibroblast GJ communication and have a crucial role in altered blood-brain-barrier permeability observed during neuroinflammation (manuscript under preparation).

Recent findings show that astrocytic Cx43 not only forms GJIC between astrocytes by Cx43/Cx43 channels, but also with oligodendrocytes by Cx43/Cx47 channels (46). Cx43/Cx47 mediated GJIC have a crucial role in maintaining oligodendrocytic K+ buffering and nutrient homeostasis (3). Moreover, Cx43 has been shown to control Cx47 phosphorylation and stability in GJs, and the loss of Cx43 may result in the secondary loss of Cx47 (32). According to a recent study on MS, disruption of Cx43/Cx47 mediated GJIC is hypothesized to be a mechanism by which demyelinating plaques expand (47). Our study was extended to observe the fate of Cx47 during MHV-A59 induced neuroinflammation. It was found that Cx47 was downregulated both at acute and chronic phases of MHV-A59 infection. In contrast to Cx43 expression, which was replenished at day 30 p.i., a significant 35.83 ± 6.5% depletion was observed for Cx47 expression even at day 30 p.i. (peak of demyelination) (Fig. 10). Interestingly, it was reported that Cx47 expression is very dynamic during both development and de- or re-myelination process in adult brain (48). *In situ* immunofluorescence data here demonstrated that Cx47 was depleted around infected areas at day 5 p.i.. At day 30 p.i., Cx47 signal was lost in and around white matter regions, albeit a moderate over-expression of Cx47 was observed in thalamus.

In recent clinical investigations of MS, it was observed that oligodendrocyte GJs were lost in myelinated fibers, and astrocyte/oligodendrocyte GJ connectivity was disrupted in MS lesions. From acute to chronic phases of demyelinating disease, oligodendrocytic GJs only recover partially. In contrast, as a part of the host remyelination process, oligodendrocyte precursor cells (OPCs) are recruited and express Cx47, which appear to re-establish limited connectivity with astrocytes (49). Our study showed that the loss of Cx47 staining in white matter was associated with loss of myelin marker PLP at the chronic phase of MHV-A59 infection. The Cx47 characteristic perikayonic expression in oligodendrocyte somata and proximal processes was noticeably disrupted in the white matter regions (Fig. 12). Loss of functional Cx47 is also reported to be associated with microglial activation (34). Microglial activation and microglia induced myelin stripping are also hallmarks of MHV-A59 induced demyelination (50). MHV-A59 induced demyelination is driven by multi-mechanistic pathways including oligodendroglial and neuronal infection, death and damage, and microglial activation (50,51). Along with these factors, MHV-A59 infection in astrocytes may affect glial GJ communication. Whether the loss of panglial GJ communication plays a pivotal role in the process of myelin loss warrants further investigation.

Experimental procedures

Preparation of mixed glial cultures.

Mixed glial cultures were established from newborn mice (day 0 to 1) using a protocol described previously (52). Briefly, following removal of meninges, brain tissues were homogenized and incubated in a rocking water bath set at 37°C for 30 min in Hanks' balanced salt solution (HBSS, Gibco), containing 300µg/ml DNase I (Sigma) and 0.25% trypsin (Sigma). Enzyme-dissociated cells were triturated in presence of 0.25% of fetal bovine serum (FBS), followed by a wash and centrifugation (300 × g for 10 min). The pellet was again resuspended in HBSS and passed through a 70-µm nylon mesh. A second wash and centrifugation (300 × g for 10 min) was performed, and finally the cell-pellet was diluted with astrocyte-specific medium (Dulbecco's modified eagle medium containing 1%penicillin-streptomycin, 1%L-glutamine, and

10%FBS). Cells were plated and allowed to adhere for 1 day in a humidified CO_2 incubator at 37°C. After 24 h, all non-adherent cells were removed and fresh astrocyte-specific medium was added. Adherent cells were maintained as mixed glial culture in astrocyte-specific medium until confluence, with a medium change every 3 to 4 days.

Isolation of primary astrocytes from mixed glia.

When the mixed glia culture was observed to be confluent, the addition of new medium was stopped for 10 days to allow differential adhesion of astrocytes and microglia. To dislodge the microglia, which grow over a strongly adherent astrocyte layer, the culture flask was thoroughly agitated in an orbital incubator shaker (180 rpm for 45 min at 37°C). Weakly adherent microglia cells came off into suspension, and these cells suspended in the culture medium were removed. The remaining adherent monolayers of cells were used as enriched astrocyte cultures for further experimentation (19).

Infection of primary astrocytes with MHV-A59.

A neurotropic demyelinating strain of coronavirus, MHV-A59, was used to understand the mechanism of retention of Cx43 in the intracellular compartment, similar to previous studies (19). Primary astrocytes were infected with inoculation medium (DMEM containing 1% penicillin-streptomycin and 1% glutamine with 2% FBS) containing MHV-A59 at multiplicities of infection (MOI) of 2. Virus particles were allowed to adhere for 1 h at 37°C in a humidified CO_2 incubator. After 1 h of incubation, infected cells were maintained in astrocyte-specific medium containing 10% normal serum. Infected cultures were subjected to different studies at specified time points postinfection (p.i.).

Immunofluorescence microscopy.

Immunofluorescence studies were done according to a protocol described previously (19). For standard immunofluorescence, primary astrocytes were plated on etched glass coverslips. The cells were fixed with 4% paraformaldehyde (PFA), followed by permeabilization with phosphate-buffered saline (PBS) containing 0.5%Triton X-100. Then cells were blocked with PBS containing 0.5% TritonX-100 and 2.5% heat-inactivated goat serum (PBS-GS), and then incubated with primary antisera diluted in blocking solution for 1 h. To remove non-specifically bound antibody, cells were washed, and then labeled with secondary antisera diluted in blocking solution. Finally, the cells were washed with PBS, mounted with mounting medium containing 4=,6-diamidino-2-phenylindole (DAPI; VectaShield, Vector Laboratories), and visualized using an Axio Observer microscope with Apotome module (Carl Zeiss, Germany). Images were acquired and processed with Zen 2012 software (Carl Zeiss, Germany). The sources and dilution of primary antibodies are listed in Table 1.

Total Internal Reflection Fluorescence (TIRF) Microscopy.

Primary astrocytes were plated on uncoated glass-bottom chambers, and allowed to grow till confluence. The cells were double immunolabeled for either Cx43 and β-tubulin or β-tubulin and N-protein. Cells were counterstained with DAPI. One ml PBS was added onto the chamber, and cells were imaged with an Olympus IX83 inverted microscope with a CellTIRF system. The images were taken with a 100× 1.51 NA TIRF objective, using a 488 nm laser. Epifluorescence images were captured in parallel for blue, green and red channels using the DAPI, FITC and TRITC filter cubes. All TIRF image processing was performed with cellSens (Olympus Life Science) and ImageJ software (NIH).

Co-Immunoprecipitation.

Co-Immunoprecipitations (co-IP) were performed according to a previously described protocol (14), with minor modifications. Primary astrocytes were washed with PBS, and harvested with PBS containing protease inhibitors. Following centrifugation, cells were resuspended with PBS containing 1% Triton X-100, 1mM EDTA, 1× complete protease inhibitor (Roche, Mannheim, Germany), and phosphatase inhibitors (1 mM $NaVO_4$ and 10 mM NaF) at 4^0C. Cells were homogenized at regular intervals, and after successful lysis in non-denaturing condition, samples were centrifuged at 1000× g for 5 min at

4^0C. Then the supernatant was incubated with MagnaBind IgG beads (Thermo Fisher Scientific, Rockford, IL, USA) for 1h at 4^0C, in order to clear any protein that binds non-specifically to the beads. After pre-clearing, samples were incubated with 2-3µg of primary antibody overnight at 4^0C. The primary antibody specific MagnaBind particles were then added to the samples, and incubated for 2 h at 4^0C. The primary antibody bound MagnaBind IgG particles were isolated using a magnetic separator (Miltenyi Biotec, Tubingen, Germany). The beads were washed three times, and finally the bound material was eluted in SDS-PAGE sample buffer. Samples were boiled and separated by SDS-PAGE, transferred to PVDF, and probed for target protein by western blot, as described previously (19). The sources and dilution of primary antibodies are listed in Table 1.

Inoculation of mice.

Use of animals and all experimental procedures were reviewed and approved by Indian Institute of Science Education and Research-Kolkata (IISER-K). Animal protocols were followed according to the guidelines of the CPCSEA, India. MHV-free, 4 weeks-old, C57BL/6 mice were intracranially inoculated with 50% of the 50% lethal dose (LD50) of MHV-A59 (2,000 PFU). The mice were monitored daily for signs and symptoms of disease. Mice were mock infected with PBS-bovine serum (BSA) and were maintained in parallel. Mice were sacrificed at the peak of inflammation (day 5 p.i.) and peak of demyelination (day 30 p.i.). Brain tissues were harvested for experimentation.

Isolation of total protein from brain.

To analyze Cx47 expression *in vivo*, total protein was extracted from brain as described previously, with minor modifications (53). Brains were flash frozen in liquid N2 and immediately dissolved in PBS containing 2% SDS, 1 EDTA-free complete protease inhibitor (Roche), and phosphatase inhibitors (1 mM $NaVO_4$ and 10 mM NaF). Lysates were sonicated on ice at 30% amplitude of 30 kHz for 0.5 s interval using a Sartorius Labsonic M sonicator. Samples were centrifuged for 20 min at maximum speed at 4°C in an Eppendorf 5415 R centrifuge. Supernatants were taken and total protein content was estimated with a Pierce BCA protein assay kit (Thermo Scientific). Twenty micrograms of total protein were loaded for each sample, and they were probed for Cx47 using rabbit polyclonal anti-Cx47 antibody (table 1) as well as for an internal control, γ-actin, by Western blotting.

Tissue processing and double-label immunofluorescence of frozen sections.

Mock- and MHV-A59-infected mice (at day 5 p.i. and day 30 p.i.) were perfused transcardially with PBS, followed by cold PBS containing 4% PFA. Brains were harvested in 4% PFA for 6 h and then placed at 4°C for 4 h in 10% sucrose, followed by 30% sucrose overnight. Tissues were embedded with OCT medium (Tissue Tek, Hatfield, PA), sectioned sagitally with the help of Cryotome (Thermo Scientific) to 10 µm thickness, and mounted on charged glass slides. Immunostaining was done as described previously (54). Frozen tissue sections were washed with PBS at RT to remove cryomatrix. Tissues then were incubated for 1 h at RT with 1 M glycine in PBS to reduce nonspecific cross-linking, followed by a 10-min incubation at RT with 1 mg/ml NaBH4 in PBS to reduce autofluorescence. Slides were washed with PBS and incubated with blocking serum containing PBS with 0.5% Triton X-100 and 2.5% goat serum (GS). The sections were incubated overnight at 4°C with a primary antiserum diluted in blocking serum, washed, and subsequently incubated with secondary antiserum diluted in PBS with GS for 2 h at RT. All incubations were carried out in a humidified chamber. After PBS washing, sections were mounted with DAPI containing mounting medium and were imaged using a Zeiss confocal microscope (LSM710), as specified. The images were processed with ImageJ software.

Statistical analysis.

All values shown are mean values ± SD (standard deviation of the means), and each data is represented as a point in the scatter plots. Student's unpaired t test was used to validate significance between two-groups and the tests were two tailed. Kruskal-Wallis ANOVA was performed for multiple group comparison in colocalization studies, after which pairwise

comparisons were made using the *post hoc* Manny-Whitney U test for multiple testing. For all experiments, statistical significance was set at P <0.05.

Acknowledgements

This work was supported by Research Grant (BT/PR14260/MED/30/437/2010 and BT/PR4530/MED/30/715/2012) from Department of Biotechnology, India, Research Grant (RG3774A2/1) from National Multiple Sclerosis Society (NMSS), USA and Indian Institute of Science Education and Research-Kolkata (IISER-K), India start up Fund to JDS. We thank Council for Scientific and Industrial research (CSIR), India and DuPre Grant from Multiple Sclerosis International Federation (MSIF) for providing the research support to RB and IISER-K IPhD Program for supporting AB. Authors thank IISER-K apoptome and confocal facility and Mr. Ritabrata Ghosh for his apoptome and confocal microscopy assistance. Authors also thank Dr. Bidisha Sinha and Ms. Arikta Biswas for TIRF facility (which is supported by Wellcome Trust DBT-India Alliance, grant no IA/I/13/1/500885) and assistance in TIRF imaging. We also thank Kenneth S. Shindler for critically reading and editing the manuscript.

Conflict of interest

The authors declare that they have no conflicts of interest with the contents of this article.

Author contributions

Rahul Basu designed and performed the experiments, analyzed the data and wrote the manuscript. Abhishek Bose performed the experiments and analyzed the data. Deepthi Thomas performed the analysis of the data and assisted in rewriting of the manuscript. Jayasri Das Sarma JDS led all aspects of this work including experimental design, participated in or supervised all experimental procedures, analyzed and interpreted data and critically revised the manuscript.

References

1. Das Sarma, J., Wang, F., and Koval, M. (2002) Targeted gap junction protein constructs reveal connexin-specific differences in oligomerization. *The Journal of biological chemistry* **277**, 20911-20918
2. Iacobas, D. A., Urban-Maldonado, M., Iacobas, S., Scemes, E., and Spray, D. C. (2003) Array analysis of gene expression in connexin-43 null astrocytes. *Physiological genomics* **15**, 177-190
3. Lutz, S. E., Zhao, Y., Gulinello, M., Lee, S. C., Raine, C. S., and Brosnan, C. F. (2009) Deletion of astrocyte connexins 43 and 30 leads to a dysmyelinating phenotype and hippocampal CA1 vacuolation. *The Journal of neuroscience : the official journal of the Society for Neuroscience* **29**, 7743-7752
4. Sofroniew, M. V., and Vinters, H. V. (2010) Astrocytes: biology and pathology. *Acta neuropathologica* **119**, 7-35
5. Charles, A. C., Merrill, J. E., Dirksen, E. R., and Sanderson, M. J. (1991) Intercellular signaling in glial cells: calcium waves and oscillations in response to mechanical stimulation and glutamate. *Neuron* **6**, 983-992
6. Charles, A. C., Naus, C. C., Zhu, D., Kidder, G. M., Dirksen, E. R., and Sanderson, M. J. (1992) Intercellular calcium signaling via gap junctions in glioma cells. *The Journal of cell biology* **118**, 195-201
7. Finkbeiner, S. (1992) Calcium waves in astrocytes-filling in the gaps. *Neuron* **8**, 1101-1108

8. Saez, J. C., Connor, J. A., Spray, D. C., and Bennett, M. V. (1989) Hepatocyte gap junctions are permeable to the second messenger, inositol 1,4,5-trisphosphate, and to calcium ions. *Proceedings of the National Academy of Sciences of the United States of America* **86**, 2708-2712
9. Tabernero, A., Giaume, C., and Medina, J. M. (1996) Endothelin-1 regulates glucose utilization in cultured astrocytes by controlling intercellular communication through gap junctions. *Glia* **16**, 187-195
10. Naus, C. C., Bechberger, J. F., Zhang, Y., Venance, L., Yamasaki, H., Juneja, S. C., Kidder, G. M., and Giaume, C. (1997) Altered gap junctional communication, intercellular signaling, and growth in cultured astrocytes deficient in connexin43. *Journal of neuroscience research* **49**, 528-540
11. Giaume, C., and McCarthy, K. D. (1996) Control of gap-junctional communication in astrocytic networks. *Trends in neurosciences* **19**, 319-325
12. Dermietzel, R., Gao, Y., Scemes, E., Vieira, D., Urban, M., Kremer, M., Bennett, M. V., and Spray, D. C. (2000) Connexin43 null mice reveal that astrocytes express multiple connexins. *Brain research. Brain research reviews* **32**, 45-56
13. Lauf, U., Giepmans, B. N., Lopez, P., Braconnot, S., Chen, S. C., and Falk, M. M. (2002) Dynamic trafficking and delivery of connexons to the plasma membrane and accretion to gap junctions in living cells. *Proceedings of the National Academy of Sciences of the United States of America* **99**, 10446-10451
14. Shaw, R. M., Fay, A. J., Puthenveedu, M. A., von Zastrow, M., Jan, Y. N., and Jan, L. Y. (2007) Microtubule plus-end-tracking proteins target gap junctions directly from the cell interior to adherens junctions. *Cell* **128**, 547-560
15. Giepmans, B. N., Verlaan, I., Hengeveld, T., Janssen, H., Calafat, J., Falk, M. M., and Moolenaar, W. H. (2001) Gap junction protein connexin-43 interacts directly with microtubules. *Current biology : CB* **11**, 1364-1368
16. Crow, D. S., Beyer, E. C., Paul, D. L., Kobe, S. S., and Lau, A. F. (1990) Phosphorylation of connexin43 gap junction protein in uninfected and Rous sarcoma virus-transformed mammalian fibroblasts. *Molecular and cellular biology* **10**, 1754-1763
17. Koster-Patzlaff, C., Hosseini, S. M., and Reuss, B. (2007) Persistent Borna Disease Virus infection changes expression and function of astroglial gap junctions in vivo and in vitro. *Brain research* **1184**, 316-332
18. Fatemi, S. H., Folsom, T. D., Reutiman, T. J., and Sidwell, R. W. (2008) Viral regulation of aquaporin 4, connexin 43, microcephalin and nucleolin. *Schizophrenia research* **98**, 163-177
19. Basu, R., Banerjee, K., Bose, A., and Das Sarma, J. (2016) Mouse Hepatitis Virus Infection Remodels Connexin43-Mediated Gap Junction Intercellular Communication In Vitro and In Vivo. *Journal of virology* **90**, 2586-2599
20. Pasick, J. M., Kalicharran, K., and Dales, S. (1994) Distribution and trafficking of JHM coronavirus structural proteins and virions in primary neurons and the OBL-21 neuronal cell line. *Journal of virology* **68**, 2915-2928
21. Biswas, K., and Das Sarma, J. (2014) Effect of microtubule disruption on neuronal spread and replication of demyelinating and nondemyelinating strains of mouse hepatitis virus in vitro. *Journal of virology* **88**, 3043-3047
22. Mingo, R. M., Han, J., Newcomb, W. W., and Brown, J. C. (2012) Replication of herpes simplex virus: egress of progeny virus at specialized cell membrane sites. *Journal of virology* **86**, 7084-7097
23. Hollinshead, M., Rodger, G., Van Eijl, H., Law, M., Hollinshead, R., Vaux, D. J., and Smith, G. L. (2001) Vaccinia virus utilizes microtubules for movement to the cell surface. *The Journal of cell biology* **154**, 389-402
24. Yea, C., Dembowy, J., Pacione, L., and Brown, M. (2007) Microtubule-mediated and microtubule-independent transport of adenovirus type 5 in HEK293 cells. *Journal of virology* **81**, 6899-6908

25. Kelkar, S. A., Pfister, K. K., Crystal, R. G., and Leopold, P. L. (2004) Cytoplasmic dynein mediates adenovirus binding to microtubules. *Journal of virology* **78**, 10122-10132
26. Xiao, P. J., and Samulski, R. J. (2012) Cytoplasmic trafficking, endosomal escape, and perinuclear accumulation of adeno-associated virus type 2 particles are facilitated by microtubule network. *Journal of virology* **86**, 10462-10473
27. Das Sarma, J. (2010) A mechanism of virus-induced demyelination. *Interdisciplinary perspectives on infectious diseases* **2010**, 109239
28. Lavi, E., Gilden, D. H., Wroblewska, Z., Rorke, L. B., and Weiss, S. R. (1984) Experimental demyelination produced by the A59 strain of mouse hepatitis virus. *Neurology* **34**, 597-603
29. Bugiani, M., Al Shahwan, S., Lamantea, E., Bizzi, A., Bakhsh, E., Moroni, I., Balestrini, M. R., Uziel, G., and Zeviani, M. (2006) GJA12 mutations in children with recessive hypomyelinating leukoencephalopathy. *Neurology* **67**, 273-279
30. Uhlenberg, B., Schuelke, M., Ruschendorf, F., Ruf, N., Kaindl, A. M., Henneke, M., Thiele, H., Stoltenburg-Didinger, G., Aksu, F., Topaloglu, H., Nurnberg, P., Hubner, C., Weschke, B., and Gartner, J. (2004) Mutations in the gene encoding gap junction protein alpha 12 (connexin 46.6) cause Pelizaeus-Merzbacher-like disease. *American journal of human genetics* **75**, 251-260
31. Orthmann-Murphy, J. L., Abrams, C. K., and Scherer, S. S. (2008) Gap junctions couple astrocytes and oligodendrocytes. *Journal of molecular neuroscience : MN* **35**, 101-116
32. May, D., Tress, O., Seifert, G., and Willecke, K. (2013) Connexin47 protein phosphorylation and stability in oligodendrocytes depend on expression of Connexin43 protein in astrocytes. *The Journal of neuroscience : the official journal of the Society for Neuroscience* **33**, 7985-7996
33. Firestone, A. J., Weinger, J. S., Maldonado, M., Barlan, K., Langston, L. D., O'Donnell, M., Gelfand, V. I., Kapoor, T. M., and Chen, J. K. (2012) Small-molecule inhibitors of the AAA+ ATPase motor cytoplasmic dynein. *Nature* **484**, 125-129
34. Tress, O., Maglione, M., Zlomuzica, A., May, D., Dicke, N., Degen, J., Dere, E., Kettenmann, H., Hartmann, D., and Willecke, K. (2011) Pathologic and phenotypic alterations in a mouse expressing a connexin47 missense mutation that causes Pelizaeus-Merzbacher-like disease in humans. *PLoS genetics* **7**, e1002146
35. Li, X., Penes, M., Odermatt, B., Willecke, K., and Nagy, J. I. (2008) Ablation of Cx47 in transgenic mice leads to the loss of MUPP1, ZONAB and multiple connexins at oligodendrocyte-astrocyte gap junctions. *The European journal of neuroscience* **28**, 1503-1517
36. Markoullis, K., Sargiannidou, I., Gardner, C., Hadjisavvas, A., Reynolds, R., and Kleopa, K. A. (2012) Disruption of oligodendrocyte gap junctions in experimental autoimmune encephalomyelitis. *Glia* **60**, 1053-1066
37. Brandizzi, F., and Barlowe, C. (2013) Organization of the ER-Golgi interface for membrane traffic control. *Nature reviews. Molecular cell biology* **14**, 382-392
38. Xu, A., Bellamy, A. R., and Taylor, J. A. (2000) Immobilization of the early secretory pathway by a virus glycoprotein that binds to microtubules. *The EMBO journal* **19**, 6465-6474
39. Ruthel, G., Demmin, G. L., Kallstrom, G., Javid, M. P., Badie, S. S., Will, A. B., Nelle, T., Schokman, R., Nguyen, T. L., Carra, J. H., Bavari, S., and Aman, M. J. (2005) Association of ebola virus matrix protein VP40 with microtubules. *Journal of virology* **79**, 4709-4719
40. Ramanathan, H. N., Chung, D. H., Plane, S. J., Sztul, E., Chu, Y. K., Guttieri, M. C., McDowell, M., Ali, G., and Jonsson, C. B. (2007) Dynein-dependent transport of the hantaan virus nucleocapsid protein to the endoplasmic reticulum-Golgi intermediate compartment. *Journal of virology* **81**, 8634-8647
41. Martin, P. E., Blundell, G., Ahmad, S., Errington, R. J., and Evans, W. H. (2001) Multiple pathways in the trafficking and assembly of connexin 26, 32 and 43 into gap junction intercellular communication channels. *Journal of cell science* **114**, 3845-3855
42. Qu, C., Gardner, P., and Schrijver, I. (2009) The role of the cytoskeleton in the formation of gap junctions by Connexin 30. *Experimental cell research* **315**, 1683-1692

43. Altevogt, B. M., and Paul, D. L. (2004) Four classes of intercellular channels between glial cells in the CNS. *The Journal of neuroscience : the official journal of the Society for Neuroscience* **24**, 4313-4323
44. Lavi, E., Suzumura, A., Hirayama, M., Highkin, M. K., Dambach, D. M., Silberberg, D. H., and Weiss, S. R. (1987) Coronavirus mouse hepatitis virus (MHV)-A59 causes a persistent, productive infection in primary glial cell cultures. *Microbial pathogenesis* **3**, 79-86
45. Arishima, H., Sato, K., and Kubota, T. (2002) Immunohistochemical and ultrastructural study of gap junction proteins connexin26 and 43 in human arachnoid villi and meningeal tumors. *Journal of neuropathology and experimental neurology* **61**, 1048-1055
46. Orthmann-Murphy, J. L., Freidin, M., Fischer, E., Scherer, S. S., and Abrams, C. K. (2007) Two distinct heterotypic channels mediate gap junction coupling between astrocyte and oligodendrocyte connexins. *The Journal of neuroscience : the official journal of the Society for Neuroscience* **27**, 13949-13957
47. Markoullis, K., Sargiannidou, I., Schiza, N., Hadjisavvas, A., Roncaroli, F., Reynolds, R., and Kleopa, K. A. (2012) Gap junction pathology in multiple sclerosis lesions and normal-appearing white matter. *Acta neuropathologica* **123**, 873-886
48. Parenti, R., Cicirata, F., Zappala, A., Catania, A., La Delia, F., Cicirata, V., Tress, O., and Willecke, K. (2010) Dynamic expression of Cx47 in mouse brain development and in the cuprizone model of myelin plasticity. *Glia* **58**, 1594-1609
49. Kleopas A. Kleopa, I. S. a. K. M. (2013) Connexin pathology in chronic multiple sclerosis and experimental autoimmune encephalomyelitis. *Clinical and Experimental Neuroimmunology* **Vol 4 (Suppl. 1)**, 45–58
50. Das Sarma, J., Kenyon, L. C., Hingley, S. T., and Shindler, K. S. (2009) Mechanisms of primary axonal damage in a viral model of multiple sclerosis. *The Journal of neuroscience : the official journal of the Society for Neuroscience* **29**, 10272-10280
51. Kenyon, L. C., Biswas, K., Shindler, K. S., Nabar, M., Stout, M., Hingley, S. T., Grinspan, J. B., and Das Sarma, J. (2015) Gliopathy of Demyelinating and Non-Demyelinating Strains of Mouse Hepatitis Virus. *Frontiers in cellular neuroscience* **9**, 488
52. Marek, R., Caruso, M., Rostami, A., Grinspan, J. B., and Das Sarma, J. (2008) Magnetic cell sorting: a fast and effective method of concurrent isolation of high purity viable astrocytes and microglia from neonatal mouse brain tissue. *Journal of neuroscience methods* **175**, 108-118
53. Ezan, P., Andre, P., Cisternino, S., Saubamea, B., Boulay, A. C., Doutremer, S., Thomas, M. A., Quenech'du, N., Giaume, C., and Cohen-Salmon, M. (2012) Deletion of astroglial connexins weakens the blood-brain barrier. *Journal of cerebral blood flow and metabolism : official journal of the International Society of Cerebral Blood Flow and Metabolism* **32**, 1457-1467
54. Das Sarma, J., Iacono, K., Gard, L., Marek, R., Kenyon, L. C., Koval, M., and Weiss, S. R. (2008) Demyelinating and nondemyelinating strains of mouse hepatitis virus differ in their neural cell tropism. *Journal of virology* **82**, 5519-5526

Figure Legends

FIG 1. Localization of Cx43 in primary astrocytes upon colchicine treatment.

Primary astrocytes were treated with 100μM colchicine for 24 h. Control cells were maintained in parallel. Cells were subjected to double-label immunofluorescence with rabbit anti-Cx43 antisera (red) and mouse anti-β-tubulin antisera (green). Z-stacking was obtained by confocal microscope from the base of the cells, at the cover slip, (plane 1) to the medial part of the cells (plane 4), to observe the distribution

of Cx43 with microtubule morphology. Untreated cells showed presence of Cx43 at both the basal (thin arrow: A) and medial parts of cells (B, C, D). In contrast, at the basal stack of colchicine treated cells (thick arrow: E), presence of Cx43 was minimal. The medial stacks showed presence of Cx43 mostly inside the cells, showing Cx43 delivery was restricted upon MT disruption, which was confirmed by disrupted β-tubulin staining (thick arrow: F, G, H). Digitally magnified insets showed that Cx43 was present on MT threads in a single focal plane and colocalization was evident, specifically where intensities of Cx43 and β-tubulin were similar (ring-like yellow spots, thin arrow: I). Colchicine-treated cells showed smear-like disrupted β-tubulin signal, whereas Cx43 surface localization was restricted (thick arrow: J).

FIG 2. Altered association of Cx43 with microtubule in primary astrocytes upon MHV-A59 infection and colchicine treatment.

Primary astrocytes were infected with MHV-A59 at an MOI of 2 or treated with 100μM colchicine for 24 h. Control cells were maintained in parallel. Cells were subjected to double-label immunofluorescence with rabbit anti-Cx43 antisera (red) and mouse anti-β-tubulin antisera (green). Cells were counterstained with DAPI (blue). In control astrocytes, punctate Cx43 (thin arrow: B) was observed to be closely associated with β-tubulin (A) and Cx43 staining was aligned along the typical radial structure of MTs (thin arrow: C).Spots of colocalized signal are shown in Panel D. Upon infection of the cells with MHV-A59, Cx43 was retained in the intracellular compartment (thick arrow: F). Although the MT morphology appeared to be normal (E), intracellular compartment retained Cx43 had a minimal association with the MT network (thick arrow: G). The intensity and number of colocalization spots were reduced (H). Upon colchicine treatment, the MT network was depolymerized in the primary astrocytes and diffuse tubulin staining was observed in the cytosol (I). Colchicine treatment showed retention of Cx43 in the intracellular compartment, predominantly in the perinuclear area (thick arrow: J, K). The number of colocalization spots was reduced significantly (L). The number of colocalization points compared between experimental groups showed there was ~ 62.8 % reduction in virus-infected cells compared to mock-infected cells (**, $P<0.01$, Mann-Whitney U test) and ~ 80.3 % reduction in colchicine-treated cells compared to mock-infected cells (**, $P<0.01$, Mann-Whiney U test). Comparison of all three groups by Kruskal-Wallis ANOVA showed differences were significant (****, $P<0.0001$, M). Five fields were analyzed for each group from N=3 experiments (K). Digitally magnified images showed Cx43 molecules were aligned along a MT thread (N, O), whereas intracellular compartment retained Cx43 did not show such alignment (P, Q). Association of Cx43 molecules on a single MT thread is shown (red line: Cx43 and green line: tubulin). Cx43 molecules showed high intensity peaks on MT threads in mock;-infected cells (R, S), but not in virus-infected cells (T, U).

FIG 3. Association of MHV-A59 virus particles with microtubules in primary astrocytes.

Primary astrocytes were infected with MHV-A59 at an MOI of 2 and mock-infected cells were maintained in parallel. Cells were subjected to double-label immunofluorescence with rabbit anti-β-tubulin antisera (red) and mouse anti-N antisera (green). Cells were counterstained with DAPI (blue) and merged image projection (mip) signals were imaged with an apotome microscope. No viral-N specific signal was observed in mock-infected cells (A) but viral-N staining was observed to be dispersed from perinuclear space to the surface of MHV-A59-infected cells (arrow: D). MT morphology is shown in mock-infected (B) and virus-infected (arrow: E) cells. MHV-A59-infected cells showed the virus specific signal colocalizing with the MTs. Specifically near the cell periphery, viral-N signal was present on MT threads (arrow: F). As expected no viral-N signal was seen in mock-infected cells (C).

FIG 4. Kinetics of viral particle spread along microtubule threads.

To observe viral spread along MT threads, primary astrocytes were mock- (A, B) or MHV-A59-infected at 6 h (C, D), 12 h (E, F), 18 h (G, H) and 24 h (I, J) p.i., cells were labeled for β-tubulin (red) and viral-N (green). The amount of anti-N staining increased from 6 h p.i. to 24 h p.i. At 6 h and 12 h p.i., discrete

viral particles were observed on MT-threads (C, E: arrow and inset) and colocalization points were mainly located at the cell periphery (D, F). At 18 h and 24 h p.i., anti-N signal was more dispersed throughout the whole cell, and towards the cell border viral particles were localized on MTs (G, I: arrow and inset). The number of colocalization points increased visually and were mainly located at the cell periphery and cell-to-cell junctions (H, J). Spots containing colocalization of signal were counted and plotted with increasing time p.i. Colocalization spots increased from 6 h p.i. to 12 to 18h p.i. and reached its maximum at 24 h p.i. (**, $P<0.01$ for each of 6 h, 12 h and 18 h p.i. and 24 h p.i. as compared with mock, Mann-Whitney U test). Kruskal-Wallis testing showed the difference was significant in a five group comparison (***, $P<0.001$). Five to six fields were analyzed for each group from N=3 experiments (K).

FIG 5. TIRF microscopy confirmed association of MT network with cortical Cx43, which was depleted due to MT/MHV-A59 interaction.

Primary astrocytes, plated on glass coverslips, were mock-infected or infected with MHV-A59 and upon staining with β-tubulin (red) and Cx43 (green), subjected to TIRF imaging to specifically capture the immunofluorescent signal of cortical Cx43. The imaging depth was limited to within 100 nm of the coverslip. Simultaneously, the whole cell MT network was imaged by epifluorescence microscopy. In control astrocytes, Cx43 (A) was observed to be closely associated with positive ends of MTs, or the MT network (B, thin arrow: C). Insets show Cx43 molecules were either precisely aligned along the MT thread (thin arrow: D) or present at the tip of the MT thread (thin arrow: E). In MHV-A59-infected cells, minimal cell surface-associated Cx43 signal was observed (F), as intracellular compartment retained Cx43 was restricted from reaching the cell surface. MT morphology appeared normal (G). As expected, in infected cells, Cx43 molecules were not associated with positive ends of MTs (thick arrow: H, I, J). Similarly, mock- and virus-infected cultures of primary astrocytes were stained for β-tubulin (red) and viral-N (green), and TIRF imaging was performed as described before. Mock-infected astrocytes showed no viral-N specific signal (K, M) and MT morphology was normal (L, M). Inset shows a digitally magnified area of mock-infected cell's periphery (N). MHV-A59-infected astrocyte cultures showed presence of viral-N staining (O, Q) and MT morphology was shown in panel P. Merged images show a pattern of viral spread at the cell surface in a single infected cell, where viral-N staining colocalized with MTs (Q). Inset shows the viral particles were aligned along the MT thread at the cell surface (R).

FIG 6. Whole cell expression of Cx43 and β-tubulin upon MHV-A59 infection.

Primary astrocytes immunolabeled for Cx43 and β-tubulin, which was subjected to TIRF microscopy were simultaneously taken for epifluorescence microscopy to obtain the whole-cell Cx43 expression. Thus, parallel epifluorescence images were captured for the same field. Cx43 was observed to be present in profuse amount as its characteristic punctate stain of Cx43 (thin arrow: A, merged: C). In contrast, MHV-A59 infected astrocytes showed mainly perinuclear localization of Cx43 (thick arrow: D, merged: F), which was not observed by TIRF imaging. MT morphology is shown for mock (B) or MHV-A59 infected cells (E). The distance of Cx43 molecules from the nucleus (distance was calculated from nuclear centroid) was measured with the help of imageJ (G). For mock infected cells Cx43 was present approximately 25.9 μm away, which was reduced to ~ 12.7μm in MHV-A59 infected cells. Data was obtained from nine different images from N= 3 biological replicates and average ± SD is represented (****, $P<0.0001$, t-test).

Fig 7. Reduction in Cx43/β-tubulin interaction in protein level upon virus infection.

Primary astrocytes were either mock-infected or infected with MHV-A59 at an MOI of 2. Proteins were extracted, followed by immunoprecipitation with monoclonal anti- β-tubulin antibody and subjected to immunoblot analysis using polyclonal anti-Cx43 antibody (detected nearly at 43 kDa). γ-actin was used as loading control (detected nearly at 42 kDa). Inputs showed reduction of total Cx43 upon MHV-A59 infection, where γ-actin expression was not altered. Upon co-IP, substantial reduction in tubulin associated Cx43 was observed in the MHV-A59-infected cells, compared to the mock-infected cells. Beads, used in preclearing, showed no signal upon probing with anti-Cx43 (A). Densitometric analysis showed that Cx43, associated with β-tubulin, was reduced ~ 44.25 % in MHV-A59 infected cells, compared to the mock-infected cells (B; ****, P<0.0001, t-test). Similarly, the virus- and mock-infected cells were co-immunoprecipitated with polyclonal anti-Cx43 antibody and probed for β-tubulin using monoclonal anti- β-tubulin antibody (detected nearly at 50 kDa). β-tubulin was expressed in equal amount in mock- and MHV-A59-infected cells. Cx43 associated β-tubulin signal was downregulated significantly in virus-infected cells (C). Densitometric analysis showed that β-tubulin, associated with Cx43, was depleted ~ 55.61 % upon virus infection (D; ****, P<0.0001, N=3, t-test).

FIG 8. Direct interaction between viral particles and β-tubulin.

To understand whether reduced Cx43/β-tubulin interaction was due to interaction between viral particle and MTs, co-IP was performed using polyclonal anti-β-tubulin antibody. The immunoprecipitated samples were probed with monoclonal anti- N antibody. Samples were probed for γ-actin, as internal control. Viral N protein was selectively detectable near 50 kDa, in the MHV-A59-infected sample only, whereas γ-actin expression was similar between mock- and virus-infected cells. MHV-A59-infected cells also showed viral N-protein directly interacted with β-tubulin. The beads which were used in preclearing, showed no specific signal upon probing with anti-Cx43.

FIG 9. Altered Cx43 localization upon inhibition of cytoplasmic dynein.

Primary astrocytes were treated with a cytoplasmic dynein inhibitor, ciliobrevin D for 24 h and DMSO treated control cells were maintained in parallel. Cells were immunolabeled for β-tubulin (green) and Cx43 (red), and nuclei were counterstained with DAPI (blue). Mock-infected cells showed prominent presence of Cx43 at the cell surface (thin arrow: A). Dose dependent treatment of ciliobrevin treatment induced aggregated localization of Cx43 around the nucleus, showing that inhibition of dynein restricted Cx43 surface localization (thick arrow: B-D).

FIG 10. Persistent loss of oligodendrocytic Cx47 in mouse whole brain protein.

C57Bl/6 mice were mock- or MHV-A59-infected and proteins were extracted from brain at day 5 p.i. (acute phase) and at day 30 p.i. (chronic phase). Whole brain proteins were probed for Cx47 (detected nearly at 47 kDa) and internal control, γ-actin (detected nearly at 42 kDa). Oligodendrocytic Cx47 was reduced in brain in the acute stage of inflammation, at day 5 p.i. (A). There was ~ 32.78 % depletion reduction (normalized with γ-actin) of Cx47 in the whole brain protein (B).The mean ± SD incidences from three different animals is shown (***, P<0.001). At the peak of demyelination at day 30 p.i., Cx47 was not replenished back to its normal level (C). Both the Cx47 immunoprobed blots showed a non-specific signal at about 51 kDa. A persistent ~ 35.83 % reduction in Cx47 expression signal was observed, upon normalization with internal control γ-actin (D, ****, P<0.0001).

FIG 11. *In situ* immunofluorescence data on infected brain tissue demonstrated sustained loss of perikaryonic Cx47 signal in MHV-A59 infected mouse brain.

Cryosections were obtained from mock- and MHV-A59-infected mouse brains at day 5 p.i. and day 30 p.i., and double-label immunofluorescence was performed for viral-N (green) and Cx47 (red). Nuclei

were stained with DAPI (blue). No virus-specific staining was observed for mock-infected brains (A, C) and prominent Cx47 staining was observed around oligodendrocytic somata (thin arrow: C, D). Characteristic perikaryonic signal of Cx47 was evident (inset: D). At day 5 p.i., MHV-A59-infected brains showed presence of viral-N signal (E, G). Loss of Cx47 signal was observed specifically around virus infected area of brain (F, thick arrow: G). Inset shows Cx47 immunostaining was disrupted (thick arrow: H). At the peak of demyelination at day 30 p.i., there was no infectious viral particle observed in brain (I, K). In contrast, disrupted Cx47 staining was noticeable in some areas of brain (J, thick arrow: K). Normal Cx47 specific signal, visible in oligodendrocytic perikariya, remained depleted at day 30 p.i. (inset, thick arrow: L). Images (with an area of 135µm × 135µm) obtained from N=3 biological replicates were quantified for presence of complete perikaryonic punctate or disrupted signal of Cx47 (M) . A reduction of perikaryonic Cx47 plaque count was observed for both at day 5 and day 30 p.i. At day 5 p.i., MHV-A59 infected mice showed ~ 7.6 Cx47 intact perikaryonic plaques reduction in an area of 135µm × 135µm (***, $P< 0.001$, t-test). At day 30 p.i., ~ 6.9 intact Cx47 plaques were reduced in an area of 135µm × 135µm (**, $P< 0.01$, t-test) (M).

FIG 12. Loss of Cx47 staining was associated with loss of PLP staining in chronic phase.

Brain sections obtained from mock- and MHV-A59-infected mice were immunolabeled for Cx47 (green) and myelin marker, PLP (red). Nuclei were counterstained with DAPI (blue). In mock-infected mice, Cx47 showed characteristic stain at oligodendrocytic perikarya, specifically in and around the white matter regions of brain e.g. corpus callosum (A, C), anterior commissure (I, K) and cerebellum (Q, S). Prominent and profuse PLP staining was observed in normal corpus callosum (B, C), anterior commissure (J, K) and cerebellum (R, S). Insets show perikaryonic Cx47 staining was observed in parallel to the PLP-stained myelinated axon fibers (thin arrow: D, L, T). MHV-A59-infected mice showed disrupted Cx47 staining, specifically in corpus callosum (E, G). Anterior commissure (M, O) and cerebellum (U, W) showed Cx47 staining, which appeared to be normal but the number of Cx47-positive puncta was marginally reduced. The loss PLP of staining was visible in specific areas of corpus callosum (F, G) but only marginal loss was evident in anterior commissure (N, O) and cerebellum (V, W). Insets show the altered expression pattern of Cx47 (thick arrow: H, P, X). Depletion of Cx47 staining was noticeably associated with loss of PLP-staining in corpus callosum (H).

Table 1. Antibodies used for immunofluorescence, co-IP and western blot

Antibodies	Dilution/ Amount used	Source
Polyclonal anti Cx43 antibody (rabbit)	Immunofluorescence: 1:200 Western blot: 1:1000	C6219, Sigma, St. Louis, MO, USA
Polyclonal anti β-tubulin antibody (rabbit)	Immunofluorescence: 1:100 Co-IP: 3µg	BB-AB0119, Biobharati LifeSciences Pvt. Ltd, Kolkata, India
Monoclonal anti β-tubulin antibody (mouse)	Immunofluorescence: 1:200 Co-IP: 2µg	Clone TUB 2.1, T4026, Sigma, St. Louis, MO, USA
Monoclonal anti Nucleocapsid (N) antibody (mouse)	Immunofluorescence: 1:50 Western blot: 1:100	Kindly provided by Dr. Julian Leibowitz
Polyclonal anti-Cx47 antibody (rabbit)	Immunofluorescence: 1:50 Western blot: 1:1000	Invitrogen Corporation, ,Camarillo, CA
Anti-proteolipid protein (PLP) antibody (rat)	Immunofluorescence: 1:1	Kindly provided by from Judith B. Grinspan (Children's Hospital of Philadelphia, Philadelphia, PA)
Secondary antibodies	As described in the text	

Figure 1.

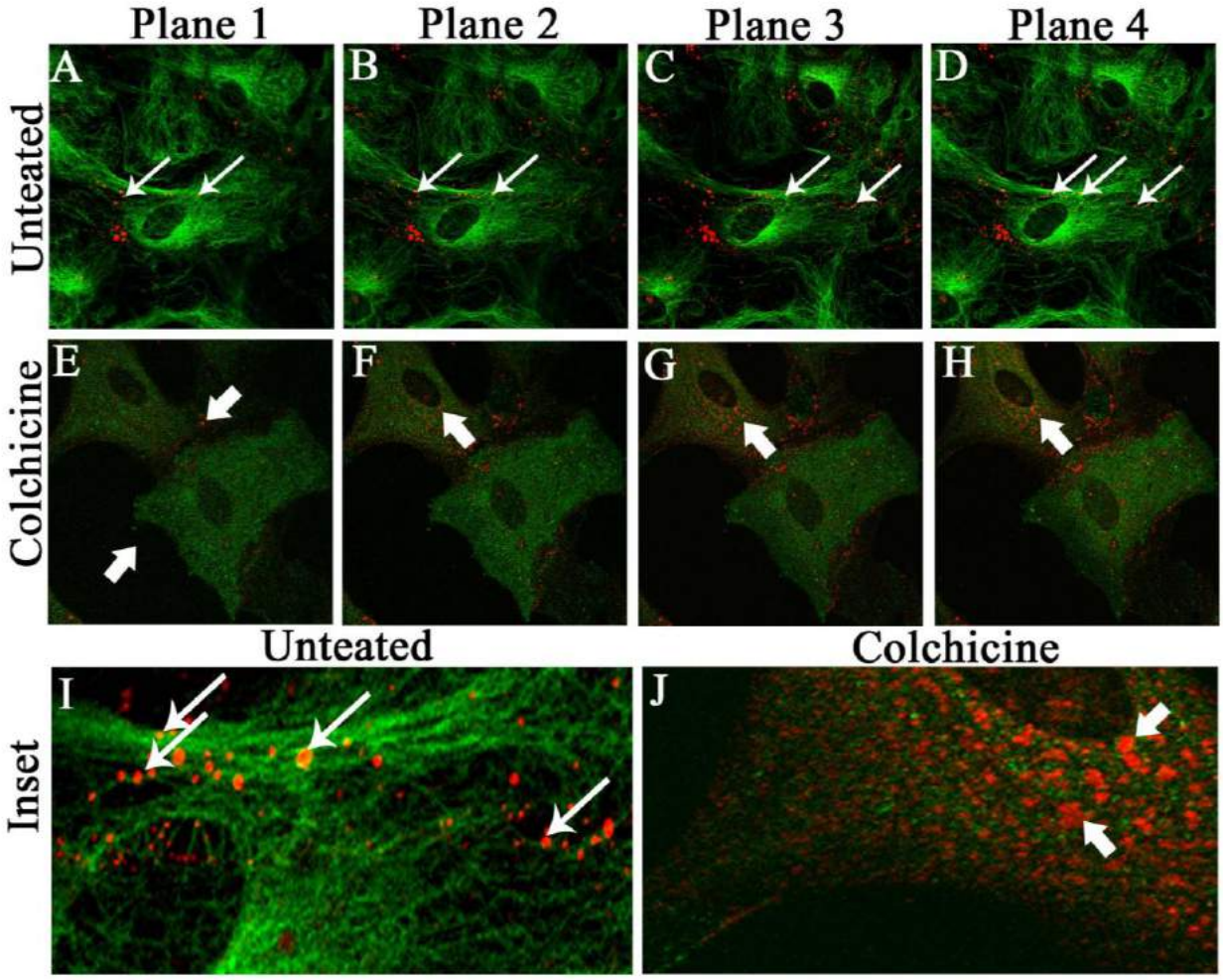

Figure 2.

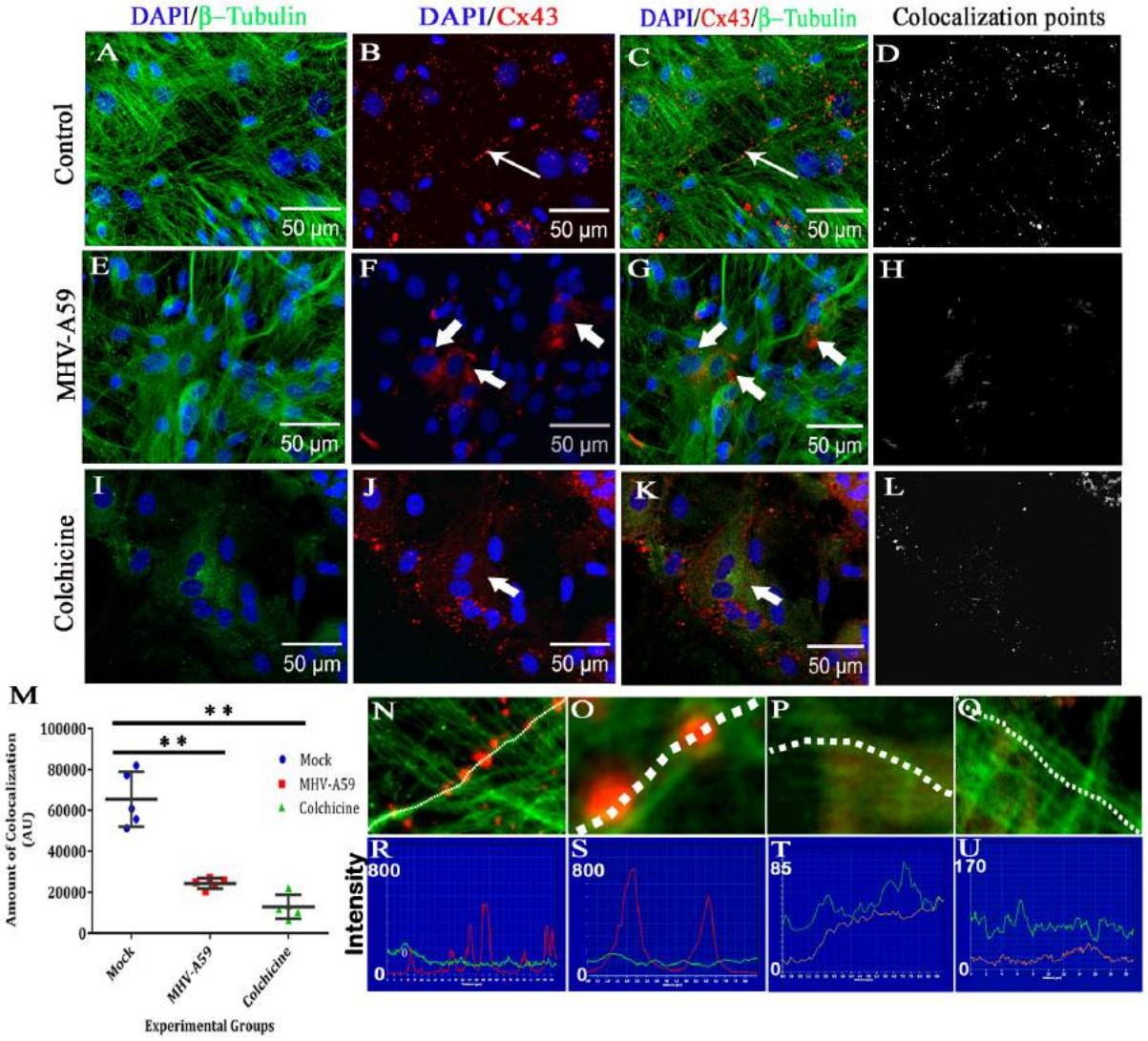

Figure 3.

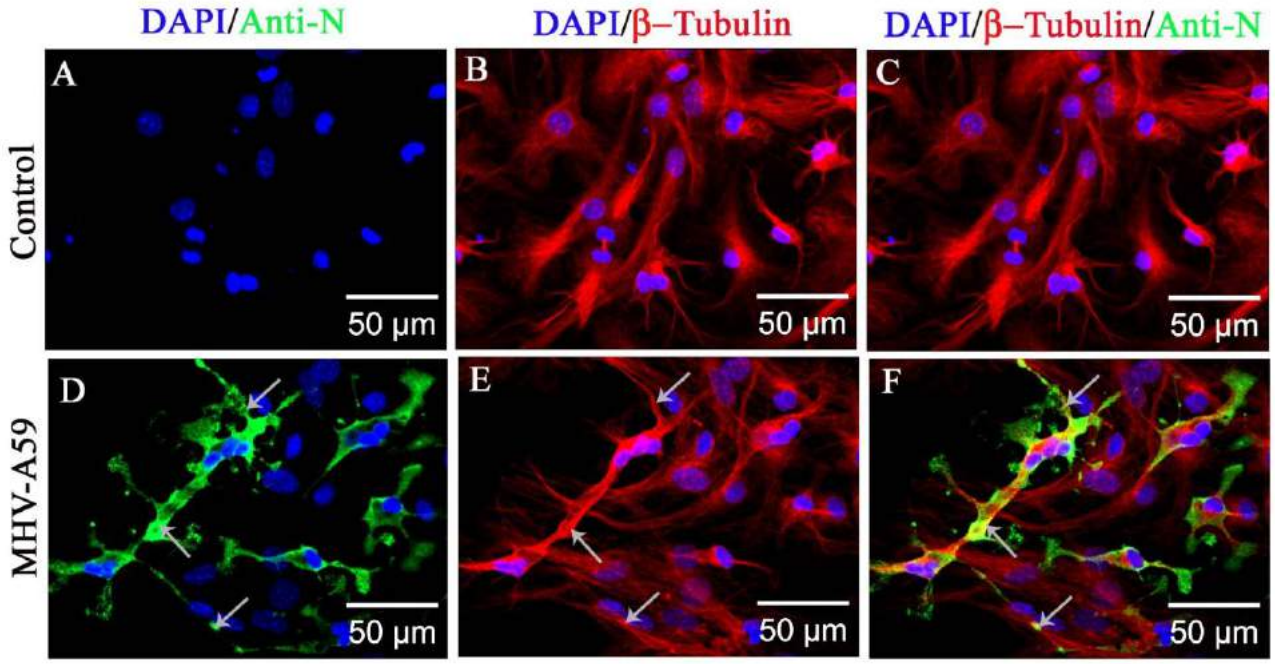

Figure 4.

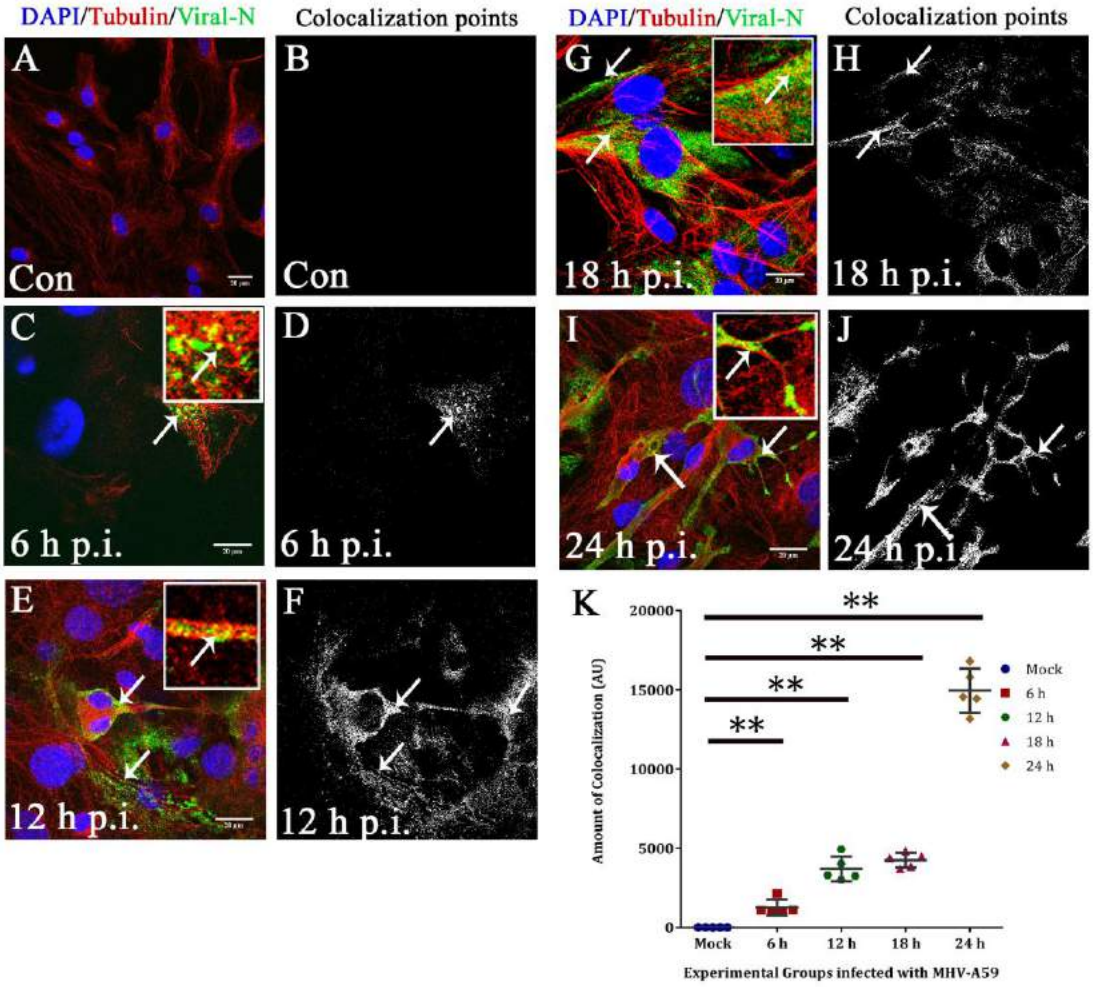

Figure 5.

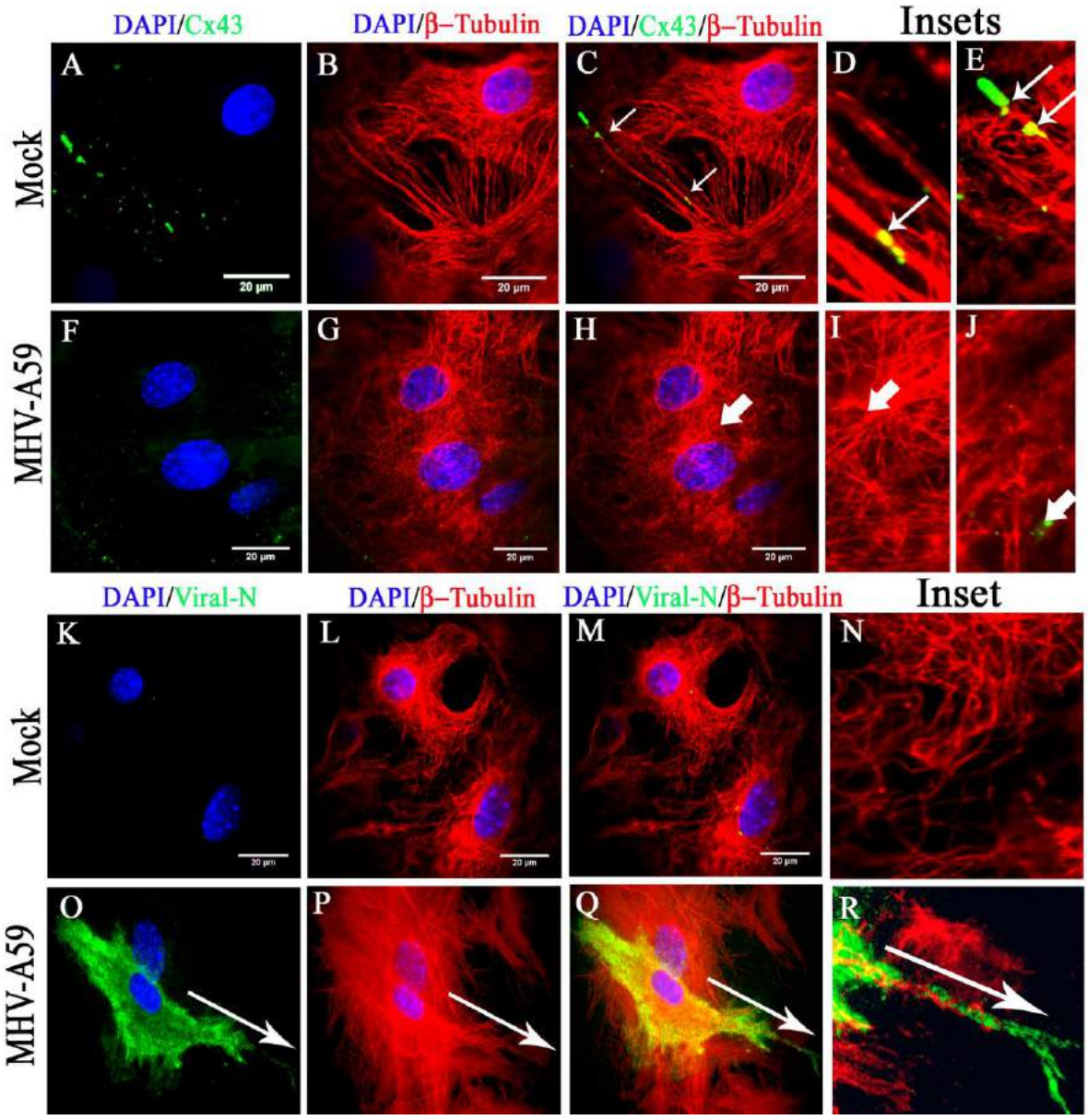

Figure 6.

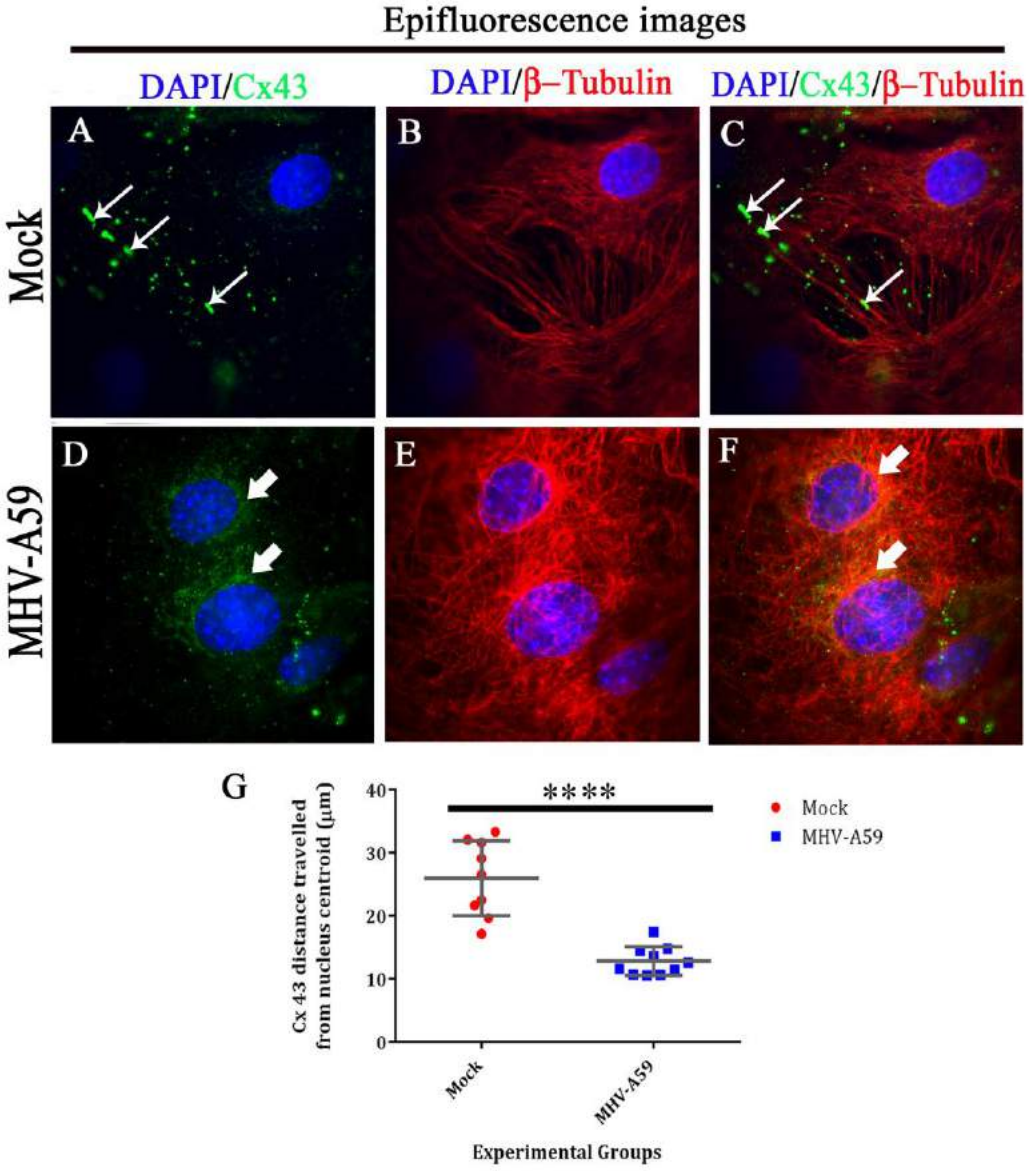

Figure 7.

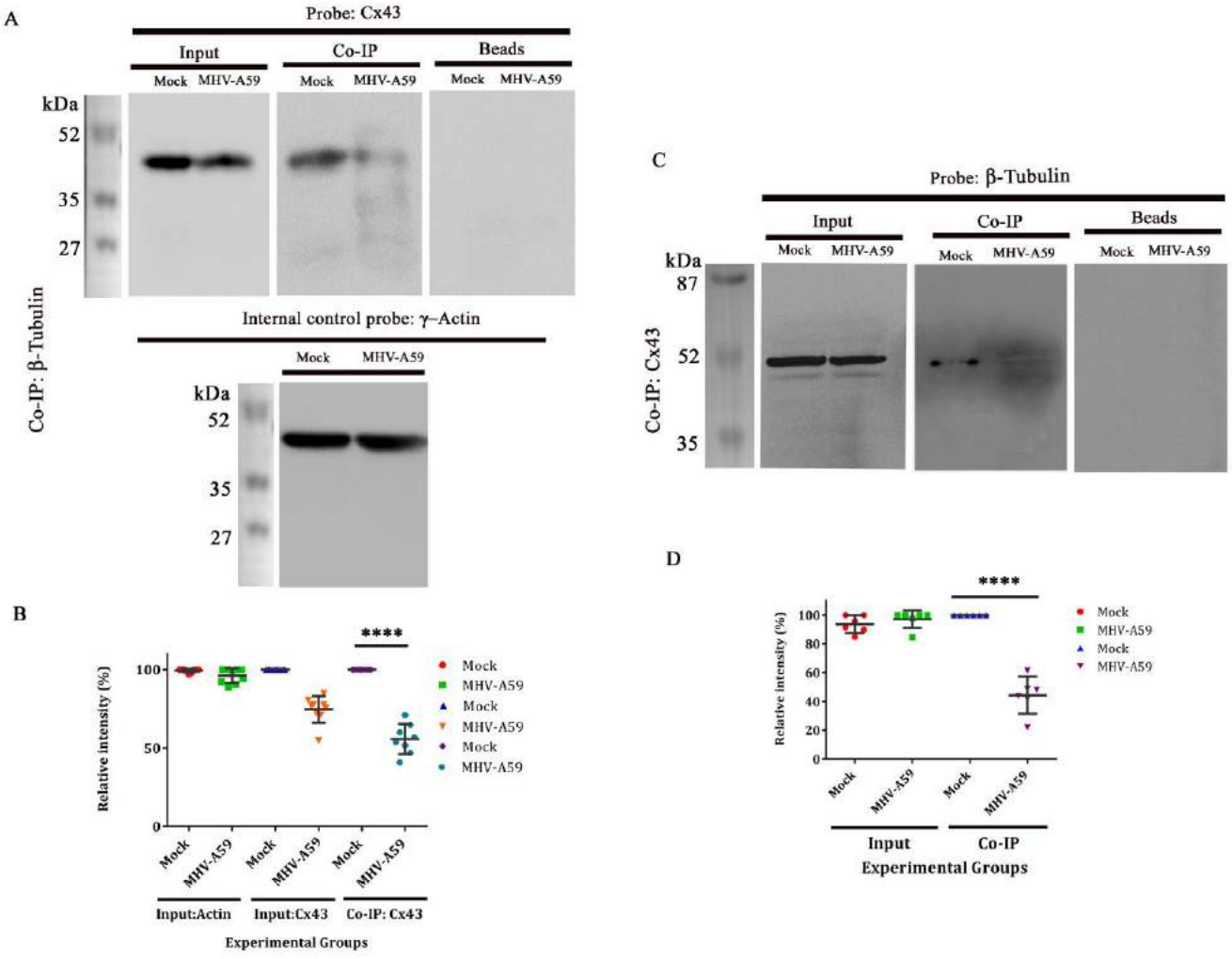

Figure 8.

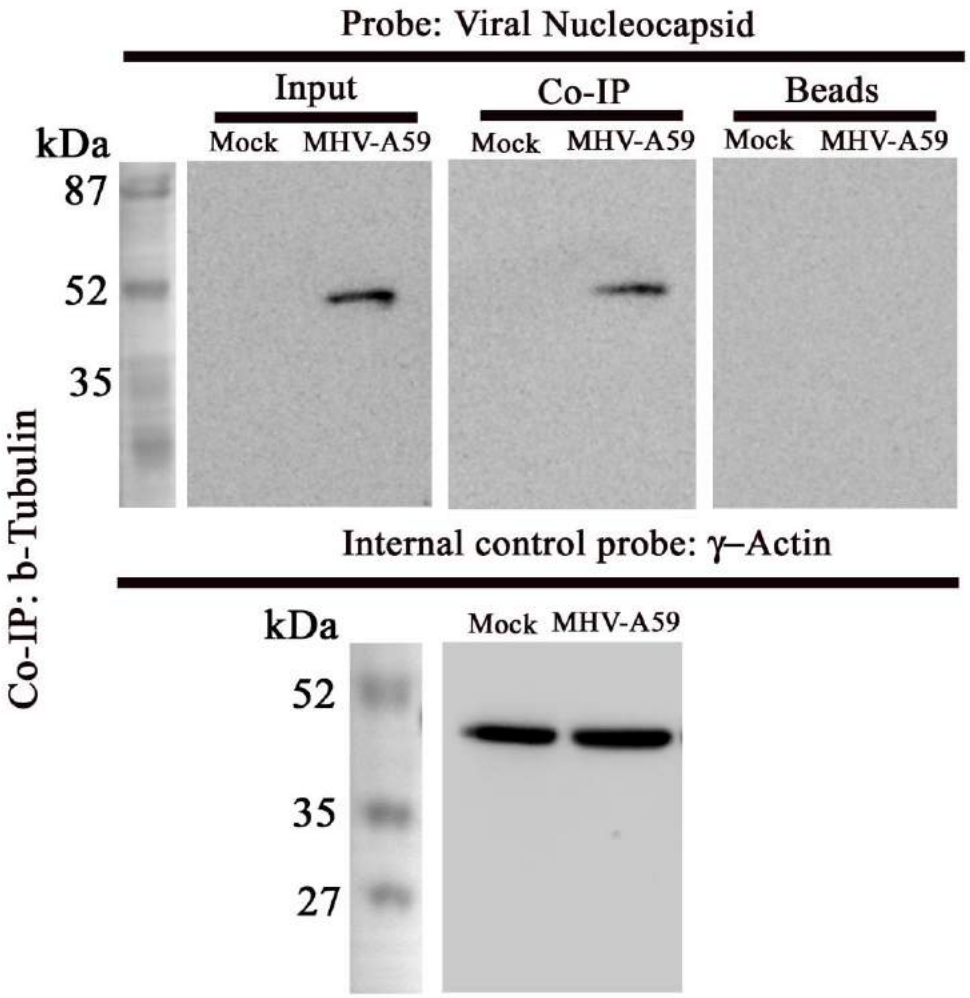

Figure 9.

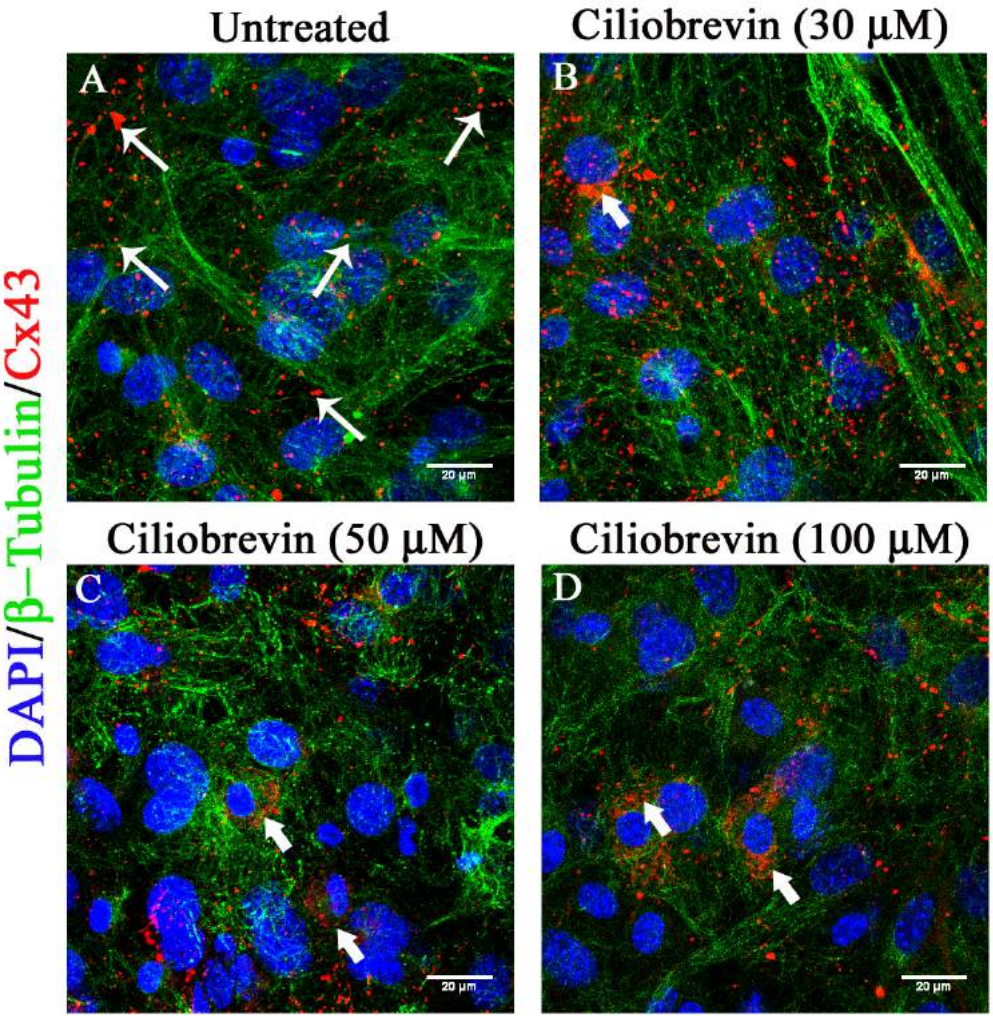

Figure 10.

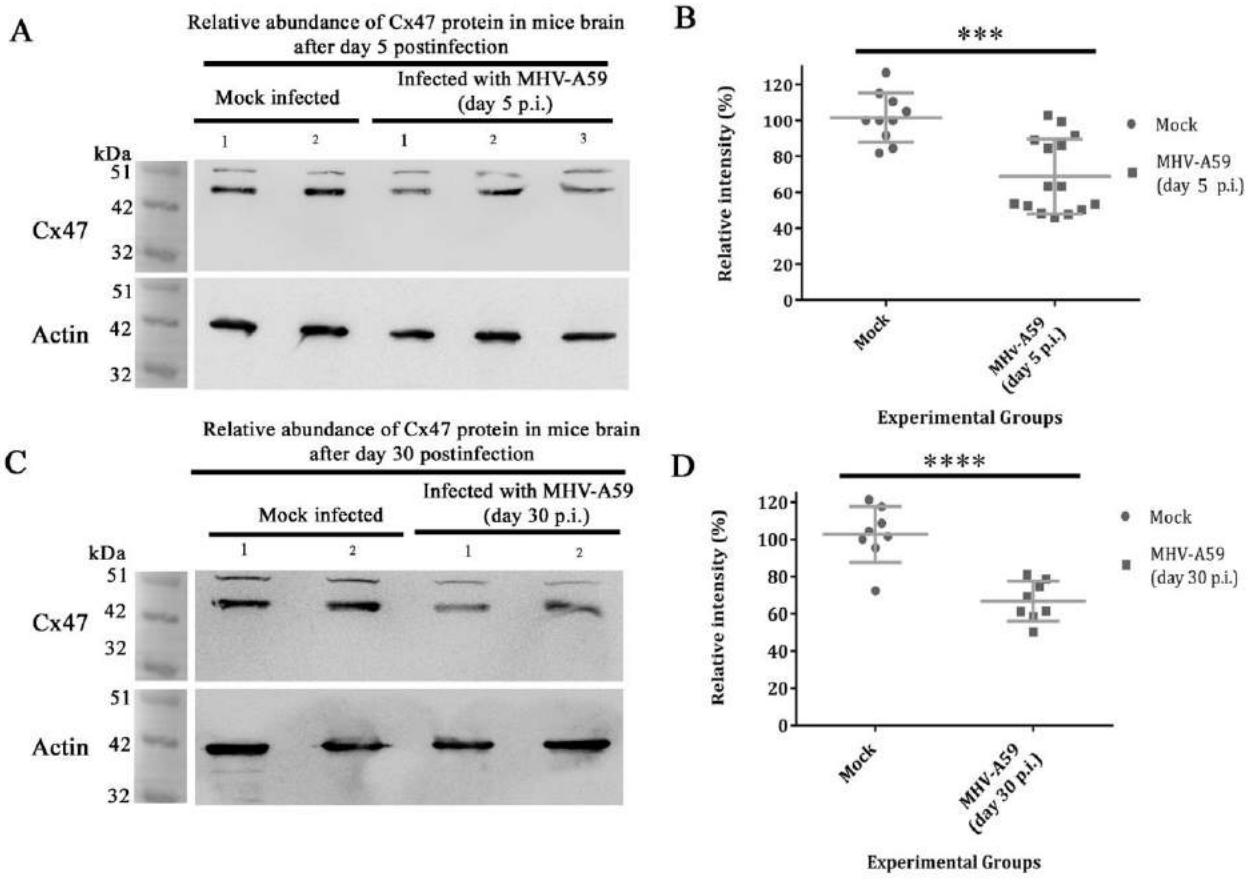

Figure 11.

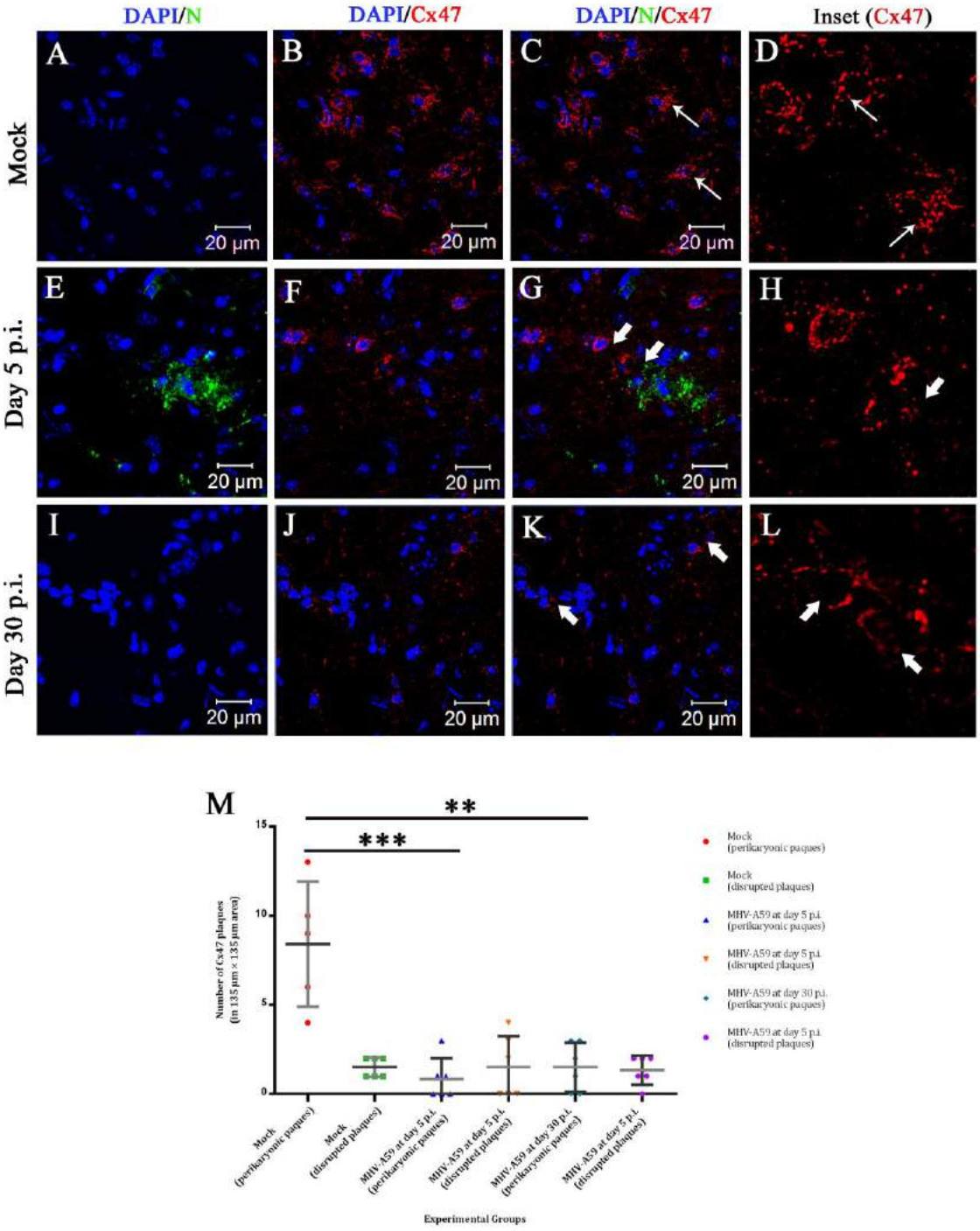

Figure 12.

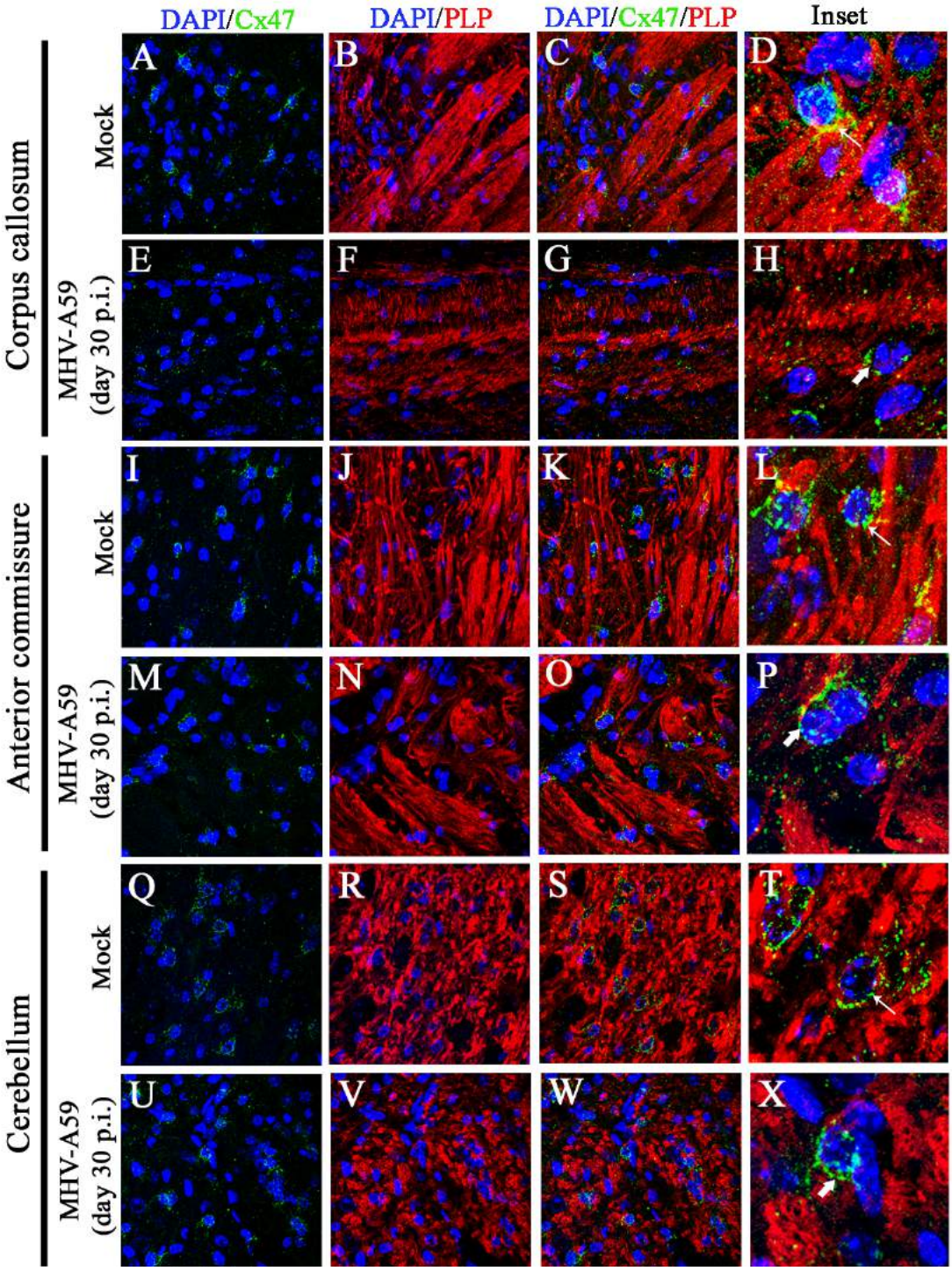

Microtubule assisted altered trafficking of Astrocytic Gap Junction Protein Connexin 43 is associated with depletion of Connexin 47 during Mouse Hepatitis Virus infection

Rahul Basu, Abhishek Bose, Deepthi Thomas and Jayasri Das Sarma

J. Biol. Chem. published online May 31, 2017